AD-A055 263 GRUMMAN AEROSPACE CORP BETHPAGE N Y F/G 20/4
AN AUTOMATED PROCEDURE FOR COMPUTING THE THREE-DIMENSIONAL TRAN--ETC(U)
FEB 77 J NASH, R SCRUGGS F33615-75-C-3073
UNCLASSIFIED AFFDL-TR-77-122-VOL-3 NL

| OF |
AD
A055 263

END
DATE
FILMED
7-78
DDC

A055109
V. 2, App A

AFFDL-TR-77-122
VOLUME III

V. 2 - A054 998

AN AUTOMATED PROCEDURE FOR COMPUTING THE THREE DIMENSIONAL TRANSONIC FLOW OVER WING-BODY COMBINATIONS, INCLUDING VISCOUS EFFECTS

VOLUME III
AN IMPLICIT METHOD FOR THE CALCULATION OF THREE DIMENSIONAL BOUNDARY LAYERS ON FINITE, THICK WINGS

SYBUCON, INC.
1900 THE EXCHANGE
ATLANTA, GEORGIA 30339

UNDER SUBCONTRACT TO:

GRUMMAN AEROSPACE CORPORATION
BETHPAGE, NEW YORK 11714

FEBRUARY 1977

TECHNICAL REPORT AFFDL-TR-77-122, VOLUME III
FINAL REPORT FOR PERIOD 1 MAY 1975 - 1 OCTOBER 1977

AIR FORCE FLIGHT DYNAMICS LABORATORY
AIR FORCE WRIGHT AERONAUTICAL LABORATORIES
AIR FORCE SYSTEMS COMMAND
WRIGHT-PATTERSON AIR FORCE BASE, OHIO 45433

NOTICE

When Government drawings, specifications, or other data are used for any purpose other than in connection with a definitely related Government procurement operation, the United States Government thereby incurs no responsibility nor any obligation whatsoever; and the fact that the government may have formulated, furnished, or in any way supplied the said drawings, specifications, or other data, is not to be regarded by implication or otherwise as in any manner licensing the holder or any other person or corporation, or conveying any rights or permission to manufacture, use, or sell any patented invention that may in any way be related thereto.

Approved for public release; distribution unlimited.

This technical report has been reviewed and is approved for publication.

J. Kenneth Johnson
Project Engineer

Dr. Thomas M. Weeks
Supervisor

FOR THE COMMANDER

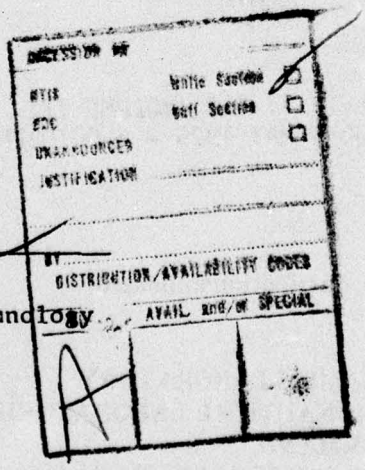

Alfred C. Draper
Assistant for Research and Technology
Aeromechanics Division

Copies of this report should not be returned unless return is required by security considerations, contractual obligations, or notice on a specific document.

AIR FORCE/56780/21 April 1978 — 150

SECURITY CLASSIFICATION OF THIS PAGE (When Data Entered)

REPORT DOCUMENTATION PAGE

READ INSTRUCTIONS BEFORE COMPLETING FORM

1. REPORT NUMBER: AFFDL-TR-77-122, VOLUME III	2. GOVT ACCESSION NO.
3. RECIPIENT'S CATALOG NUMBER: TR-77-122-VOL-3	
4. TITLE (and Subtitle): AN AUTOMATED PROCEDURE FOR COMPUTING THE THREE-DIMENSIONAL TRANSONIC FLOW OVER WING-BODY COMBINATIONS, INCLUDING VISCOUS EFFECTS. VOLUME III. AN IMPLICIT METHOD FOR THE CALCULATION OF THREE-DIMENSIONAL BOUNDARY LAYERS ON FINITE, THICK WINGS.	5. TYPE OF REPORT & PERIOD COVERED: FINAL REPORT, MAY 1975 - OCTOBER 1977
	6. PERFORMING ORG. REPORT NUMBER
7. AUTHOR(s): JOHN NASH, ROY SCRUGGS	8. CONTRACT OR GRANT NUMBER(s): F33615-75-C-3073
9. PERFORMING ORGANIZATION NAME AND ADDRESS: GRUMMAN AEROSPACE CORPORATION, BETHPAGE, NEW YORK 11714 *	10. PROGRAM ELEMENT, PROJECT, TASK AREA & WORK UNIT NUMBERS: PROGRAM ELEMENT 62201F, PROJECT 1476, TASK 147601, WORK UNIT 14760127
11. CONTROLLING OFFICE NAME AND ADDRESS: AIR FORCE FLIGHT DYNAMICS LABORATORY, WRIGHT-PATTERSON AIR FORCE BASE, OHIO 45433	12. REPORT DATE: FEBRUARY 1978
	13. NUMBER OF PAGES: 95
14. MONITORING AGENCY NAME & ADDRESS (if different from Controlling Office)	15. SECURITY CLASS. (of this report): UNCLASSIFIED
	15a. DECLASSIFICATION/DOWNGRADING SCHEDULE

16. DISTRIBUTION STATEMENT (of this Report)

Approved for public release; distribution unlimited.

17. DISTRIBUTION STATEMENT (of the abstract entered in Block 20, if different from Report)

Final rept. 1 May 75 - 1 Oct 77.

18. SUPPLEMENTARY NOTES

* UNDER SUBCONTRACT BY: SYBUCON INC.
1900 THE EXCHANGE, SUITE 175
ATLANTA, BEORGIA 30339

19. KEY WORDS (Continue on reverse side if necessary and identify by block number)

VISCOUS FLOWS
THREE-DIMENSIONAL BOUNDARY LAYERS
AIRCRAFT AERODYNAMICS
COMPUTATIONAL FLUID DYNAMICS

20. ABSTRACT (Continue on reverse side if necessary and identify by block number)

This volume contains the theory and description of the code of a new three-dimensional boundary layer program that computes the laminar and turbulent boundary layers over finite thick wings.

DD FORM 1 JAN 73 1473 EDITION OF 1 NOV 65 IS OBSOLETE

SECURITY CLASSIFICATION OF THIS PAGE (When Data Entered)

FOREWORD

This final report was prepared by the Aerodynamics Section of the Grumman Aerospace Corporation, Bethpage, New York for the Flight Mechanics Division, Air Force Flight Dynamics Laboratory, Wright-Patterson Air Force Base, Ohio. The work was performed under Contract No. F33615-75-C-3073, which was initiated under Project No. 1476, "Advanced Wing-Body Aerodynamic Analysis and Design." Mr. J. Kenneth Johnson (FXM) was the Project Monitor of this contract.

The report consists of three volumes. Volume I, entitled "Description of Analysis Methods and Applications," describes the methods used to predict surface pressure distributions and aerodynamic forces on three-dimensional wing-body combinations at transonic speeds, including viscous effects. Volume I also contains an extensive set of comparisons between numerical predictions and experimental results. Detailed instructions required to use the program are provided in Volume II, "User's Manual and Code Description." Volume III was written at Sybucon, Inc., Atlanta, Georgia and contains a complete description of the theory and program that computes the full three-dimensional boundary layer over the wing. This work was performed by Sybucon under subcontract to Grumman Aerospace. Although this program operates independently of the program described in Volume II, the input data set required for the full three-dimensional boundary layer computation is generated by the code documented in Volume II.

Mr. F. Berger was the Program Manager; Dr. W. Mason and Mr. D. MacKenzie served as Project Engineers. The work was performed in close cooperation with the co-authors from the NASA Ames Research Center, Dr. W. F. Ballhaus and Ms. J. Frick. Additional contributors to the project included G. Simpers, A. Vachris, D. Raila, P. Aidala, M. Sturm and A. Bunnell of Grumman, and Drs. F. R. Bailey and T. Holst of NASA Ames. Moreover, contributions have been made by A. Chen of Boeing, Drs. R. Melnik, B. Grossman and G. Volpe of the Grumman Research Department and Grumman Consultants Prof. A. Jameson, Prof. J. Werner and Dr. E. Murman. As noted above, the three-dimensional boundary layer program was written by Dr. J. Nash and Dr. R. Scruggs of Sybucon, Inc.

TABLE OF CONTENTS

LIST OF ILLUSTRATIONS

LIST OF ILLUSTRATIONS (Continued)

LIST OF SYMBOLS

C_p	pressure coefficient
F	denotes the 4 x 1 vector of dependent variables
I	identity matrix
K_{ij}	the ij^{th} component of curvature; i,j = 1,3
L_D	dissipation length
M	Mach number of maximum number of y-mesh points
Q	total velocity vector
R_{OT}	lateral rotation matrix
R_{OB}	backward rotation matrix
T	temperature
U,V,W	velocity components in the x,y,z directions respectively
X,Y,Z	airframe ordinates in the stream, vertical, and span directions respectively, forming a right-handed system
a_1, a_2	empirical turbulence parameters, defined in the text
a	speed of sound
c_p	specific heat at constant pressure
h_1, h_2, h_3	metric coefficients in x,y,z directions respectively
k	thermal conductivity
p	pressure
$\overline{q^2}$	mean square fluctuating velocity
u,v,w	fluctuating velocity components in x,y,z directions
x,y,z	local orthogonal curvilinear coordinates on body surface
Λ	sweep angle
δ	boundary layer thickness
δ^*	boundary layer displacement thickness

η	normalized coordinate normal to surface
ρ	density
τ	shear stress
μ	molecular viscosity
λ	curvilinear interpolation parameter, function of local geometry
γ	ratio of specific heats
$\gamma_{n\pm1}$	rotation angle in the z-direction for z^+ and z^- respectively
γ_b	backward rotation angle at local (x,z)-station

Subscripts:

e	edge value, edge of boundary layer
w	wall value
o	stagnation value
∞	freestream value
ℓ	node point index in x-direction
m	node point index in y-direction
n	node point index in z-direction

Superscripts:

$\hat{}$	denotes dimensional value
$\tilde{}$	denotes non-dimensional value
$\bar{}$	denotes time-averaged value

SECTION I

INTRODUCTION

1. BACKGROUND

The method described herein was developed with the objective of producing a computationally efficient scheme for calculating three-dimensional boundary layers: laminar or turbulent, over a finite swept wing of arbitrary planform and thickness, in compressible steady flow. The method is intended to be used both for routine boundary-layer calculations in specified pressure fields, and for interactive calculations in which the pressure field will be generated by a parallel potential flow calculation via suitable iterative coupling.

The approach adopted has been to draw on the extensive experience gained with the earlier turbulent methodology (References [1 through 8]), to retain the turbulence-model formulation essentially intact, and to concentrate on improving the numerical aspects of the method and its data-handling capabilities. The need for radical improvements in this latter area became evident from the large amount of hand work which had to be done in performing calculations even for the simple planform geometry considered in References [6,7]. It was subsequently decided to upgrade the basic fluid-dynamic package by including the thermal energy equation, in differential form, among the governing equations, so as to provide greater generality for the method. It was also decided to avoid the limitations, imposed by matching the solution to a separate inner-layer calculation near the wall, by continuing the numerical solution through the viscous sublayer. Lastly, the provision for performing purely laminar calculations, near the leading edge or elsewhere, was to be made.

As far as the numerical scheme was concerned, it was thought essential to replace the explicit formulation, used in the earlier methods, by an implicit one. Only by doing so would it be possible for the user to gain control over the chordwise step length and escape from the excessive computer run-times which had been typical at high Reynolds numbers. On the other hand, the adoption of an implicit numerical scheme posed a number of problems which had not arisen with the older explicit method. First, the long chordwise step lengths, made possible by the implicit scheme, and the need to scan the integration domain laterally, presented problems in proper treatment of the zones of dependence. These problems were resolved by using an alternating direction technique, which offered other advantages too. Second, the implicit formulation of the particular set of governing equations, which included the empirically-modified turbulent kinetic-energy equation, posed stability problems associated with changing character of the equations: the equations become hyperbolic near the wall whereas (since molecular viscosity is included) they are parabolic in the outer part of the flow. The stability problems were resolved by representing the turbulent dissipation as a sink term in the matrix form of the governing equations.

2. OUTLINE OF THE METHOD

The wing surface is segmented into quasi-quadrilateral panels (Figure 1) and a locally orthogonal set of curvilinear coordinates is constructed following a conical development of the local region. The development is required to satisfy certain geometrical constraints. Streamwise cuts are made over the planform at arbitrary spanwise locations and the number of surface points on each cut is the same. The

calculation then proceeds from the planform leading edge; proper account being taken as to whether the leading edge is turbulent or laminar. The governing equations are finite-differenced with respect to the local surface normal coordinate y, and the locally transverse coordinate z, so that in the local y-z plane the difference equations are implicit. The solution is then obtained at each x (streamwise) station in succession. This chordwise forward-marching is applied with arbitrary step length proceeding from leading to trailing edge or until separation is encountered at some spanwise location. Provision is made to step past locally separating regions if desired. Transition from laminar to turbulent flow may be triggered at the user's discretion at any chordwise position, except when the leading edge flow is already turbulent.

SECTION II

GOVERNING EQUATIONS

The following equations relate to a steady, compressible, three-dimensional turbulent boundary layer developing on a doubly-curved surface of large radii.

1. COORDINATE SYSTEM

The equations are expressed in terms of a coordinate system: x,y,z, that is precisely orthogonal on the surface: $y = 0$, on which the boundary layer is developing, and approximately orthogonal elsewhere, to within a tolerance compatible with the customary first-order boundary-layer approximations (Figure 2). The metric coefficients, associated with the x-, y-, z-directions, are h_1, h_2, h_3, respectively, and curvature parameters of the form

$$K_{13} = \frac{1}{h_1 h_3} \frac{\partial h_1}{\partial z} \tag{2.1}$$

$$K_{31} = \frac{1}{h_1 h_3} \frac{\partial h_3}{\partial x} \tag{2.2}$$

$$K_{21} = \frac{1}{h_1 h_2} \frac{\partial h_2}{\partial x} \tag{2.3}$$

$$K_{22} = \frac{1}{h_2^2} \frac{\partial h_2}{\partial y} \tag{2.4}$$

$$K_{23} = \frac{1}{h_2 h_3} \frac{\partial h_2}{\partial z} \tag{2.5}$$

satisfy the appropriate Lame relationships [4,9].

2. EQUATIONS OF MOTION

The velocity components, corresponding to x,y,z, are expressed as

$U + u$, $V + v$, $W + w$, respectively, where U, V, W are defined as time-averaged means, and u, v, w are the instantaneous fluctuations about those means. Similarly, the static temperature, pressure, and density are expressed as $T + \phi$, $p + p'$, $\rho + \rho'$, respectively.

The equations of motion: consisting of the two mean-flow momentum equations, the mean thermal-energy equation, and the continuity equation, can accordingly be written in the form

$$\frac{\rho U}{h_1}\frac{\partial U}{\partial x} + \frac{1}{h_2}(\rho V + \overline{\rho' v})\frac{\partial U}{\partial y} + \frac{\rho W}{h_3}\frac{\partial U}{\partial z}$$

$$+ \rho W(K_{13}U - K_{31}W) + \frac{1}{h_1}\frac{\partial p}{\partial x}$$

$$+ \frac{1}{h_2}\frac{\partial}{\partial y}(\rho\overline{uv}) - \frac{1}{h_2}\frac{\partial}{\partial y}\left(\frac{\mu}{h_2}\frac{\partial U}{\partial y}\right) = 0 , \qquad (2.6)$$

$$\frac{\rho U}{h_1}\frac{\partial W}{\partial x} + \frac{1}{h_2}(\rho V + \overline{\rho' v})\frac{\partial W}{\partial y} + \frac{\rho W}{h_3}\frac{\partial W}{\partial z}$$

$$- \rho U(K_{13}U - K_{31}W) + \frac{1}{h_3}\frac{\partial p}{\partial z}$$

$$+ \frac{1}{h_2}\frac{\partial}{\partial y}(\rho\overline{vw}) - \frac{1}{h_2}\frac{\partial}{\partial y}\left(\frac{\mu}{h_2}\frac{\partial W}{\partial y}\right) = 0 , \qquad (2.7)$$

$$\frac{\rho U c_p}{h_1}\frac{\partial T}{\partial x} + \frac{c_p}{h_2}(\rho V + \overline{\rho' v})\frac{\partial T}{\partial y} + \frac{\rho W c_p}{h_3}\frac{\partial T}{\partial z}$$

$$- \frac{U}{h_1}\frac{\partial p}{\partial x} - \frac{W}{h_3}\frac{\partial p}{\partial z} - \frac{1}{h_2}\frac{\partial}{\partial y}\left(\frac{k}{h_2}\frac{\partial T}{\partial y}\right)$$

$$- \frac{\mu}{h_2^2}\left\{\left(\frac{\partial U}{\partial y}\right)^2 + \left(\frac{\partial W}{\partial y}\right)^2\right\} + \rho\varepsilon + \frac{c_p}{h_2}\frac{\partial}{\partial y}(\rho\overline{v\phi}) = 0 \qquad (2.8)$$

$$\frac{1}{h_1}\frac{\partial}{\partial x}(\rho U) + \frac{1}{h_2}\frac{\partial}{\partial y}(\rho V + \overline{\rho' v}) + \frac{1}{h_3}\frac{\partial}{\partial z}(\rho W)$$

$$+ \rho U(K_{21} + K_{31}) + \rho W(K_{13} + K_{23}) = 0 \ , \qquad (2.9)$$

where ε is the rate of turbulent dissipation into heat.

In Equations (2.6, 7, 8), μ, k and c_p are the molecular viscosity, the thermal conductivity, and the specific heat at constant pressure, respectively, and they can be related to one another via the Prandtl number: $Pr = \mu c_p/k$, which is taken to be a constant (= 0.72); c_p is also taken to be a constant (= 6006 $ft^2.sec^2\ °R$), and hence μ and k are proportional to each other. The molecular viscosity is taken to be a function of local static temperature via the Sutherland formula:

$$\mu = 2.270\ \frac{T^{3/2}}{T + 198.6} \times 10^{-8}\ \text{lb sec/ft}^2 \ . \qquad (2.10)$$

The fluid is assumed to be thermally perfect, whereupon the equation of state holds, in the form

$$p = \rho RT \qquad (2.11)$$

where the gas constant: $R = 1716\ ft^2/sec^2\ °R$. These values of c_p and R are consistent with $\gamma = 1.4$, where γ is the ratio of the specific heats.

3. CLOSURE RELATIONSHIPS

Closure of the system of equations is effected by means of the turbulent kinetic-energy equation, which is written in the form

$$\frac{\rho U}{h_1}\frac{\partial}{\partial x}\left(\frac{\overline{q^2}}{2}\right) + \frac{1}{h_2}(\rho V + \overline{\rho' v})\frac{\partial}{\partial y}\left(\frac{\overline{q^2}}{2}\right) + \frac{\rho W}{h_3}\frac{\partial}{\partial z}\left(\frac{\overline{q^2}}{2}\right) +$$

$$\frac{\rho\overline{uv}}{h_2}\frac{\partial U}{\partial y} + \frac{\rho\overline{vw}}{h_2}\frac{\partial W}{\partial y} + \frac{\rho}{h_2}\frac{\partial}{\partial y}\left(\frac{\overline{p'v}}{\rho} + \frac{\overline{q^2 v}}{2}\right) + \rho\varepsilon = 0 \ , \qquad (2.12)$$

where $$\overline{q^2} = \overline{u^2} + \overline{v^2} + \overline{w^2} \ , \qquad (2.13)$$

together with empirical relationships to model the diffusion and dissipation terms, and to model the dependence of the turbulent shear stresses and turbulent heat flux on $\overline{q^2}$.

Specifically, following Bradshaw et al. [10, 11] and Nash [1], the diffusion and dissipation terms are modeled, respectively by

$$\overline{p'v} + \frac{\overline{q^2 v}}{2} = \frac{\overline{q^2}_{max}}{Q_e} a_2 \overline{q^2} \qquad (2.14)$$

$$\varepsilon = - \frac{(\overline{q^2})^{3/2}}{L_D} \ , \qquad (2.15)$$

where $\overline{q^2}_{max}$ is the maximum value of $\overline{q^2}$ in the outer three-fourths of the boundary-layer, and where the diffusion function: a_2, and the dissipation length: L_D, are assumed to be universal functions of physical distance through the boundary layer. The particular forms for a_2 and L_D, used here, are the same as those found appropriate in earlier studies [3,4], and can be represented by

$$a_2 = 1.125\ \eta^2 - 0.375\ \eta^4 \qquad (2.16)$$

$$\frac{L_D}{\delta} = \frac{7.195}{1 + 4\eta^2 + 5\eta^7} \ . \qquad (2.17)$$

These two functions are illustrated in Figure 3. In Equations (2.16,17) η is the dimensionless physical distance through the boundary layer:

$$\eta = \frac{1}{\delta} \int_o^y h_2 dy \ , \qquad (2.18)$$

and δ is the boundary-layer thickness, defined as the distance from the surface where

$$\{(U_e - U)^2 + (W_e - W)^2\}^{1/2} = 0.005\, Q_e \tag{2.19}$$

The turbulent shear-stress components are related to $\overline{q^2}$ by empirical functions of the form

$$\rho\overline{uv} = -\rho\overline{q^2}\, f\left\{\frac{L_D}{(\overline{q^2})^{1/2} h_2}\frac{\partial U}{\partial y}\right\} \tag{2.20}$$

$$\rho\overline{vw} = -\rho\overline{q^2}\, f\left\{\frac{L_D}{(\overline{q^2})^{1/2} h_2}\frac{\partial W}{\partial y}\right\}. \tag{2.21}$$

Several earlier models are contained as special cases in Equations (2.20,21): If $f(\psi)$ = constant, the Townsend structural-equilibrium model [12] is recovered; if $f(\psi) \propto \psi$, the isotropic eddy viscosity model is recovered (although not a prescribed eddy viscosity) finally, if $f(\psi) \propto \psi^2$, the mixing length model is recovered. It is the intention to explore the implications of and experimental support for, alternative forms for the function f at a later date; meanwhile, a cursory study of some available experimental data (Figure 4) indicates the suitability of the form

$$f(\psi) = 0.0225\, \psi, \tag{2.22}$$

and this form has been provisionally adopted.

The corresponding relationship between turbulent heat flux and $\overline{q^2}$ is written as

$$\overline{v\phi} = - \frac{(\overline{q^2})^{3/2}}{c_p} g \left\{ \frac{c_p L_D}{\overline{q^2} h_2} \frac{\partial T}{\partial y} \right\}, \qquad (2.23)$$

where g is another empirical function. To date the various possible forms for g have not been explored, and the present work is based on the provisional form

$$g(\psi_T) = \frac{0.0225\ \psi_T}{Pr_t} \qquad (2.24)$$

in which Pr_t is an assumed constant value (= 0.9) of the turbulent Prandtl number. An obvious refinement could be to allow Pr_t to vary with position across the boundary layer.

4. DIMENSIONLESS VARIABLES

Characteristic scales of length, velocity, temperature, and density: L_o, Q_o, T_o, ρ_o, respectively, are introduced for the purposes of reducing the variables to dimensionless form. Two of these, in turn, define a Mach number, M_o, where

$$M_o = \frac{Q_o}{(\rho R T_o)^{1/2}} \qquad (2.25)$$

the particular choice of characteristic scales is of no special significance; here, Q_o is identified with the free-stream velocity, and T_o and ρ_o are associated with stagnation conditions.

The dimensionless variables subsequently become

$$\tilde{x} = \frac{x}{L_o}\ ,\ \tilde{y} = \frac{y}{L_o}\ ,\ \tilde{z} = \frac{z}{L_o} \qquad (2.26)$$

$$\tilde{U} = \frac{U}{Q_o} , \quad \tilde{V} = \frac{V}{Q_o} , \quad \tilde{W} = \frac{W}{Q_o} \tag{2.27}$$

$$\tilde{T} = \frac{T}{T_o} , \quad \tilde{\rho} = \frac{\rho}{\rho_o} , \quad \tilde{p} = \frac{p}{\rho_o Q_o^2} \tag{2.28}$$

$$\tilde{\mu} = \frac{\mu}{\rho_o Q_o L_o} , \quad \tilde{k} = \frac{k}{c_p \rho_o Q_o L_o} \tag{2.29}$$

$$\tilde{\overline{q^2}} = \frac{\overline{q^2}}{Q_o^2} , \quad \tilde{\overline{uv}} = \frac{\overline{uv}}{Q_o^2} , \quad \tilde{\overline{vw}} = \frac{\overline{vw}}{Q_o^2} \tag{2.30}$$

$$\tilde{\overline{v\phi}} = \frac{\overline{v\phi}}{Q_o T_o} . \tag{2.31}$$

In what follows, the ~ sign will be dropped for clarity, but it will be understood that the variables retain their dimensionless status as defined here.

5. EQUATIONS IN MATRIX-VECTOR FORM

The two momentum equations (Equations 2.6,7), the thermal-energy equation (Equation 2.8), and the empirically modified turbulent kinetic-energy equation (Equation 2.12) are selected as the principle governing equations, leaving the continuity equation to be solved retrospectively. These four principle governing equations can conveniently be written in matrix vector form, as follows:

$$A_1 F + A_2 \frac{\partial F}{\partial x} + A_3 \frac{\partial F}{\partial z} + A_4 \frac{\partial F}{\partial y}$$

$$+ A_5 \frac{\partial^2 F}{\partial y^2} + A_6 = 0 , \tag{2.32}$$

where F is a four-dimensional vector of the principle dependent variables:

$$F^T = \{U, W, T, \overline{q^2}\} \ . \tag{2.33}$$

In Equation (2.32) the A_1 through A_5 are 4 x 4 matrices, and A_6 is a 4-dimensional vector.

A_2 and A_3 are simply products of a scalar with the identity matrix, I, of order 4:

$$A_2 = \frac{\rho U}{h_1} I, \quad A_3 = \frac{\rho W}{h_3} I \ ; \tag{2.34}$$

A_5 is a diagonal matrix, and A_4 is full. A_1 could contain off-diagonal terms, depending on the particular formulation; here it contains only one term, as indicated below.

Writing

$$A_1 = [a_{(1)i,j}] \tag{2.35}$$

$$h_2 A_4 = [a_{(4)i,j}] \tag{2.36}$$

$$h_2^2 A_5 = [a_{(5)i,j}] \tag{2.37}$$

$$A_6 = \{a_{(6)i}\} \ , \tag{2.38}$$

the non-zero content of these matrices is as follows:

$$a_{(1)4,4} = \frac{2}{L_D} (\overline{q^2})^{1/2} \ , \tag{2.39}$$

$$a_{(4)1,1} = \rho V - m_u (c_\ell - K_{22}) + K_{22}\mu \ , \tag{2.40}$$

$$a_{(4)1,3} = -\frac{\rho\overline{q^2}}{T} f_u \,, \tag{2.41}$$

$$a_{(4)1,4} = \rho f_u \,, \tag{2.42}$$

$$a_{(4)2,2} = \rho V - m_w(c_\ell - K_{22}) + K_{22}\mu \,, \tag{2.43}$$

$$a_{(4)2,3} = \frac{\rho\overline{q^2}}{T} f_w \,, \tag{2.44}$$

$$a_{(4)2,4} = \rho f_w \,, \tag{2.45}$$

$$a_{(4)3,3} = V - m_T(c_\ell - K_{22}) + K_{22}k - (\gamma - 1)M_o^2 \frac{\rho(\overline{q^2})^{3/2}}{T} g \,, \tag{2.46}$$

$$a_{(4)3,4} = \frac{3}{2}\rho(\gamma - 1)M_o^2 (\overline{q^2})^{1/2} g \,, \tag{2.47}$$

$$a_{(4)4,1} = 2\rho\,\overline{q^2} f_u \,, \tag{2.48}$$

$$a_{(4)4,2} = 2\rho\,\overline{q^2} f_w \,, \tag{2.49}$$

$$a_{(4)4,4} = \rho V + \frac{2\rho\,\overline{q^2}_{max}\, a_2}{Q_e} \tag{2.50}$$

$$a_{(5)1,1} = -(\mu + m_u) \,, \tag{2.51}$$

$$a_{(5)2,2} = -(\mu + m_w) \,, \tag{2.52}$$

$$a_{(5)3,3} = -(k + m_T) \,, \tag{2.53}$$

$$a_{(6)1} = \rho W(K_{13}U - K_{31}W) + \frac{1}{h_1}\frac{\partial p}{\partial x}$$

$$- \frac{1}{h_2}\frac{\partial U}{\partial y}\{\frac{c_\mu \mu}{h_2}\frac{\partial T}{\partial y} - \frac{m_u}{2h_2}\overline{q^2}\frac{\partial}{\partial y}(\overline{q^2})\}\ , \qquad (2.54)$$

$$a_{(6)2} = -\rho U(K_{13}U - K_{31}W) + \frac{1}{h_3}\frac{\partial p}{\partial z}$$

$$- \frac{1}{h_2}\frac{\partial W}{\partial y}\{\frac{c_\mu \mu}{h_2}\frac{\partial T}{\partial y} - \frac{mw}{2}\frac{\partial}{\partial y}(\overline{q^2})\}\ , \qquad (2.55)$$

$$a_{(6)3} = -(\gamma-1)M_o^2\{\frac{U}{h_1}\frac{\partial p}{\partial x} + \frac{W}{h_3}\frac{\partial p}{\partial z}\}$$

$$+ \frac{\rho}{L_D}(\overline{q^2})^{3/2} + \frac{\mu}{h_2^2}\{(\frac{\partial U}{\partial y})^2 + (\frac{\partial W}{\partial y})^2\}$$

$$- \frac{1}{h_2}\frac{\partial T}{\partial y}\{\frac{c_k k}{h_2}\frac{\partial T}{\partial y} - \frac{m_T}{2h_2}\frac{\partial}{\partial y}(\overline{q^2})\}\ , \qquad (2.56)$$

$$a_{(6)4} = \frac{2\rho(\overline{q^2})_{max}\,\overline{q^2}\,c_a a_2}{Q_e h_2} \qquad (2.57)$$

where

$$m_u = -\rho(\overline{q^2})^{1/2} L_D f_u'\ , \qquad (2.58)$$

$$m_w = -\rho(\overline{q^2})^{1/2} L_D f_w'\ , \qquad (2.59)$$

$$m_T = -\rho(\overline{q^2})^{1/2} L_D g'\ , \qquad (2.60)$$

$$c_a = \frac{1}{a_2 h_2}\frac{\partial a_2}{\partial y}\ , \qquad (2.61)$$

$$c_\ell = \frac{1}{L_D h_2}\frac{\partial L_D}{\partial y}\ , \qquad (2.62)$$

$$c_\mu = \frac{1}{\mu h_2} \frac{\partial \mu}{\partial y} , \tag{2.63}$$

$$c_k = \frac{1}{k h_2} \frac{\partial k}{\partial y} . \tag{2.64}$$

In the above equations, f', g' denote differentiation with respect to their arguments; the subscripts: u, w are attached to f, f' to distinguish between the arguments involving $\partial U/\partial y$ and $\partial W/\partial y$, respectively.

6. BOUNDARY CONDITIONS

The boundary conditions on the surface over which the boundary layer is developing, which is assumed to be a smooth, impervious, thermally insulated wall, are:

$$U = V = W = 0 \tag{2.65}$$

$$\partial T/\partial y = 0 \tag{2.66}$$

$$\overline{q^2} = 0 \tag{2.67}$$

At the outer edge of the boundary layer the appropriate conditions are:

$$\frac{\partial U}{\partial y} = \frac{\partial W}{\partial y} = \frac{\partial T}{\partial y} = 0 \tag{2.68}$$

$$\overline{q^2} = 0 . \tag{2.69}$$

Initial conditions, at the leading edge, are assumed to conform to the similarity relationships pertaining to asymptotic, attachment-line flow at the local leading-edge sweep angle. Under such conditions the boundary layer quantities may be expressed in the form

$$F = F(y, C^*, M_e) \ , \tag{2.70}$$

where F is the vector dependent variable (Equation (2.33), M_e is the local external Mach number, and C^* is the similarity parameter

$$C^* = \rho_w W_{e_p}^2 / (\mu_w \partial U_{e_n} / \partial x_n) \ , \tag{2.71}$$

in which W_{e_p} is the external velocity component parallel to the attachment line U_{e_n} is the component normal to it, and x_n is the normal distance from the attachment line, measured along the wing contour. The flow in the boundary layer, on the attachment line, is considered to be laminar (at least for $M_e = 0$) if $C^* < 10^5$ (see Reference [13]), and turbulent if $C^* > 10^5$.

In the present work, the functional form, corresponding to Equation (2.70), is initially taken to be the same as its incompressible equivalent, and subsequently is improved upon via an iteration involving conditions at the first two chordwise stations. The incompressible form for laminar flow is tabulated in the text books (see, e.g., Reference [14]), and experimental results for incompressible flow are given in References [13]).

Boundary conditions must also be specified along the sides of the integration domain: i.e. for the extreme values of z, which correspond to the root and tip of the wing. The true conditions along these boundaries are, of course, unspecified and the most that can be done is to provide the user with options, representing stereotyped boundary conditions, permitting sensitivity studies to be carried out for the particular configuration and pressure distribution. Candidate stereotyped

root and tip conditions considered here are:

(a) two-dimensional flow

(b) plane-of-symmetry flow

(c) infinite-yawed-wing flow.

In each case, different assumptions are made concerning the spanwise derivatives on the boundaries, and these assumptions take the place of detailed information about the flow quantities being convected across those boundaries.

7. DISPLACEMENT THICKNESS AND WALL SHEAR STRESS

The displacement thickness: δ^*, in a three-dimensional flow (Reference [4,15]), can be determined by matching the normal component of mass flux, in the real flow, to that which would exist in a hypothetical inviscid flow about a displacement surface whose distance from the wall is δ^*. In this equivalent inviscid flow:

$$\rho_e V = \frac{\rho_e U_e}{h_1}\frac{\partial \delta^*}{\partial x} + \frac{\rho_e W_e}{h_3}\frac{\partial \delta^*}{\partial z} + \int_{y_D}^{y} \frac{\partial}{\partial y}(\rho_e V_e)dy \ , \qquad (2.72)$$

where $\partial(\rho_e V_e)/\partial y$ is given by the continuity equation (Equation 2.9):

$$-\frac{1}{h_2}\frac{\partial}{\partial y}(\rho_e V_e) = \frac{1}{h_1}\frac{\partial}{\partial x}(\rho_e U_e) + \frac{1}{h_3}\frac{\partial}{\partial z}(\rho_e W_e) + \rho_e U_e(K_{21} + K_{31}) + \rho_e W_e(K_{13} + K_{23}), \qquad (2.73)$$

and y_D is the value of y corresponding to δ^*. Upon substitution into Equation (2.72), we have

$$\rho_e V + \int_{y_D}^{y} (\rho_e U_e K_{21} + \rho_e W_e K_{23}) h_2 dy$$

$$= \frac{\rho_e U_e}{h_1} \frac{\partial \delta^*}{\partial x} + \frac{\rho_e W_e}{h_3} \frac{\partial \delta^*}{\partial z}$$

$$- \frac{1}{h_1} \frac{\partial}{\partial x} (\rho_e U_e) + \frac{1}{h_3} \frac{\partial}{\partial z} (\rho_e W_e)$$

$$+ \rho_e U_e K_{31} + \rho_e W_e K_{32} \int_{y_D}^{y} h_2 dy \qquad (2.74)$$

in which the integral on the right-hand side represents the physical distance between y_D and y. The left-hand side is set equal to the value of

$$\rho_e V + \int_{o}^{y} (\rho U K_{21} + \rho W K_{23}) h_2 dy \ .$$

determined retrospectively from the boundary-layer calculation at each x-z station, whereupon Equation (2.74) reduces to a partial-differential equation for δ^*. It is integrated over the two-dimensional domain: x,z, subject to the same side boundary conditions as were imposed on the principal governing equations.

The components of the wall shear stress, or skin friction, are determined retrospectively from the boundary-layer velocity profiles. Specifically:

$$\tau_{w_x} = \mu_w (\partial U / \partial y) \qquad (2.75)$$

$$\tau_{w_z} = \mu_w (\partial W / \partial y) \ , \qquad (2.76)$$

where μ_w is the molecular viscosity at the wall.

Separation of the boundary layer is deemed to occur when the component of the wall shear stress, normal to the local sweep line, falls to zero. This interpretation of separation is consistent with the customary interpretation of oil-flow visualization pictures. Its usefulness, as a criterion of separation, clearly deteriorates as it becomes more difficult to define the sweep lines -- as on a wing of high taper, for example. Furthermore, the more three-dimensional the flow becomes, the less certainty there is that surface-flow diagnostics correlate with the behavior of the flow in the outer part of the boundary layer; it is the angle between the external streamlines and the body surface which controls the departure of the pressure distribution and loading from their inviscid counterparts. The proper definition of separation, from an engineering standpoint, should therefore focus on abrupt changes of this streamline angle, rather than on conditions near the wall. Unfortunately there is, as yet, no agreed-upon criterion of separation which reflects this more realistic focus; the conventional wall-shear-stress criterion has therefore been adopted as a surrogate.

SECTION III

GEOMETRY REPRESENTATION

Several approaches are available for representing the body surface in terms of general curvilinear coordinate systems. The present authors take the view, however, that orthogonal systems are best suited to boundary-layer calculations because the governing equations, so formulated, preserve the physical clarity which is essential to proper description and modeling of the flow. The system chosen here is based on local development of the surface as defined by a set of airframe reference coordinates X, Y, Z. A conical development is performed at each surface mesh point as depicted in Figure 5. The figure shows the arrangement of surface mesh points on an arbitrary body in the neighborhood of point A, about which a local development is to be made. The developments are performed row-wise, marching in the general direction of the freestream. This procedure will be discussed later. Of interest for the development at A are the points B through F, of which points C through E lie generally "upstream" of A.

The lengths AB, AC, AD, AE, and AF are preserved in the development. In addition the spatial angles between adjacent pairs of directed line segments are preserved, so that local surface areas are approximately preserved as well. Figure 6(a) depicts the development of the region shown in Figure 5. The conical development generates radii of curvature r_1 and r_2, corresponding to the regions on the left and right hand sides of point A. The appropriate coordinate system is then polar, with the neighboring mesh points located via a radius, r, and an angle, θ. The origin of coordinates is fixed by a line θ = constant passing through the points B and C for the left side and E and F for the right side. The

two coordinate systems are thus arranged so that point A lies at $(r_1, 0)$ and $(r_2, 0)$ respectively. This arrangement has the desirable feature that vector quantities at point A do not require rotation in passing from one coordinate system to the other. Local vectors $\overline{AB}$, $\overline{AC}$, and so on, are generated from the input ordinate data. The appropriate distances $|AB|$ through $|AF|$ are generated by inner products such as

$$|AB| = \sqrt{\overline{AB} \cdot \overline{AB}} \quad , \tag{3.1}$$

and the angles are obtained as,

$$\delta_1 = \cos^{-1} \frac{\overline{AB} \cdot \overline{AC}}{|AB||AC|} \tag{3.2}$$

$$\delta_2 = \cos^{-1} \frac{\overline{AC} \cdot \overline{AD}}{|AC||AD|} \tag{3.3}$$

$$\delta_3 = \cos^{-1} \frac{\overline{AD} \cdot \overline{AE}}{|AD||AE|} \tag{3.4}$$

$$\delta_4 = \cos^{-1} \frac{\overline{AE} \cdot \overline{AF}}{|AE||AF|} \quad . \tag{3.5}$$

The local coordinates (r_1, θ_1) and (r_2, θ_2) are then generated by extending lines BC and EF to intersection with line DA extended. Figure 5(b) depicts a local development in the nomenclature appropriate to the finite differencing scheme used in the governing equations. The quantity λ on the left and on the right, is computed for each local development once the coordinates of points B and F are determined. The region to the left of point A is taken to be in the direction of increasing

ordinate z. All geometrical quantities can then be referred to as "+" subscripted on the side of increasing z and "-" on the decreasing side. In the finite difference equations the various geometric coefficients may now be identified from the local development:

$$h_1 = |\overline{DA}| \tag{3.6}$$

$$h_3^+ = r_1\theta_{1_B} \tag{3.7}$$

$$h_3^- = r_2\theta_{2_F} \tag{3.8}$$

$$K_{13}^+ = 1/r_1 \tag{3.9}$$

$$K_{13}^- = 1/r_2 \ . \tag{3.10}$$

As the implicit finite difference equations are developed along the span at each downstream station, it becomes necessary to form first z-derivatives of the velocity components at every point along the span. The situation is depicted in terms of the local z-differencing index n, in Figure 7. The figure depicts the development at point n of the + and - regions. Also shown are the appropriate developments for points (n-1) and (n+1). It is clear from the figure that, for example, the components U_{n-1}, W_{n-1}, computed in the frame of reference at station (n-1) can not simply be transferred to the frame of reference at position n without taking account of the relative rotation between the two frames of reference. Thus in forming z-differences of velocity at station n involving velocity at station (n-1) the angle,

$$\gamma_{n-1} = \theta_{2n} - \theta_{1_{n-1}} \tag{3.11}$$

must be used to rotate the velocity vector from station (n-1). Scalar quantities are not affected so that the four-vector $F_{n-1} = (U, W, T, \overline{q^2})^T_{n-1}$ occurring in the difference equations is given in the local frame by

$$F_{n-1} = R_{OT} \cdot F_{n-1} \tag{3.12}$$

where

$$R_{OT} = \begin{bmatrix} \cos \gamma_{n-1} & -\sin \gamma_{n-1} & 0 & 0 \\ \sin \gamma_{n-1} & \cos \gamma_{n-1} & 0 & 0 \\ 0 & 0 & 1 & 0 \\ 0 & 0 & 0 & 1 \end{bmatrix} \tag{3.13}$$

A similar rotation matrix applies when the z-derivative at n involves values at (n+1).

A similar situation exits when transferring vectors in the x-direction. Figure 8a shows a different view of the development region around point A. Recognizing that the point D was, for the previous x-step, the point about which development was performed, it is seen that a streamwise rotation may exist between the two coordinate systems. Since the only quantity needed to transfer from point D to point A is the relative rotation of the two systems, it is sufficient to construct a tangent plant at point D and to perform rotations into this plane. To fix matters, the rotation of the planes containing $\overline{DD'}$ and $\overline{DA}$ is performed about the local sweep line in the tangent plane. The result is

depicted in Figure 8b. The heavy lines depict the vector distances as seen normal to the tangent plane. The dashed lines are the result of rotation into the tangent plane. The angles γ_d and γ_a are then obtained by forming a vector along the sweep line, $\overline{CE}$, and computing the dot products,

$$\overline{D'D} \cdot \overline{CE} = |\overline{D'D}||\overline{CE}| \cos(\tfrac{\pi}{2} + \gamma_d) \tag{3.14}$$

$$\overline{AD} \cdot \overline{CE} = |\overline{AD}||\overline{CE}| \cos(\tfrac{\pi}{2} - \gamma_a) \tag{3.15}$$

The required rotation angle is then

$$\gamma_b = \gamma_a - \gamma_d \, , \tag{3.16}$$

when the streamwise slope of the tangent plane is positive, and

$$\gamma_b = \gamma_d - \gamma_a \, , \tag{3.17}$$

when the streamwise slope of the tangent plane is negative.

Then in order to transfer F at ℓ-1 to the coordinate system at ℓ, the following rotation is performed,

$$F_{\ell-1} = R_{OB} \cdot F_{\ell-1} \tag{3.18}$$

where

$$R_{OB} = \begin{bmatrix} \cos\gamma_b & \sin\gamma_b & 0 & 0 \\ -\sin\gamma_b & \cos\gamma_b & 0 & 0 \\ 0 & 0 & 1 & 0 \\ 0 & 0 & 0 & 1 \end{bmatrix} \tag{3.19}$$

All the geometric quantities discussed in this section are independent of the solution procedure once the computing stations have been settled upon. Thus for a particular wing the geometry need only be computed once, and then stored appropriately. The data are called back one spanwise row at a time as the solution progresses over the chord.

SECTION IV

NUMERICAL SCHEME

The governing equations are solved, by an implicit finite-difference method, erected upon the surface on which the boundary layer is developing. A forward-marching procedure is adopted, advancing in some direction: x, in which the mean velocity component is everywhere non-negative.

1. ITERATION PROCEDURE

The matrix-vector equation (Equation 2.32), representing the four principal governing equations, is nonlinear because the coefficient matrices depend on F. Accordingly, the customary local linearization approach is employed, involving an iteration procedure which successively updates coefficient matrices until they are consistent with the converged values of F at the station where the solution is being sought. Flow charts of the iteration procedure are shown in the Appendix.

The external flow is solved first, to provide converged values of U_e, W_e, in terms of the local pressure coefficient: C_p. For this purpose Equation (2.32), which degenerates to a partial-differential equation in only two independent variables: x,z, is integrated implicitly along a line of roughly constant x. The values of U_e, W_e produced are then used to scale the first-guess solution within the boundary layer.

Within the boundary layer, Equation (2.32) is integrated by means of an alternating-direction implicit (ADI) method, covering each successive cross-plane of roughly constant x. The ADI method is embedded within an iteration loop, again, for the purpose of updating the coefficient matrices to a status consistent with the final solution: F. The

continuity equation is also integrated, within this iteration loop, to provide current values of the effective normal mass flux: $\rho V + \overline{\rho' v}$.

2. DIFFERENCE APPROXIMATIONS

The integration mesh is configured such that the forward-marching procedure advances along lines of constant y and z. Accordingly, if ℓ, m, n denote indexing in the x-, y-, z-directions, respectively (Figure 9), x-derivatives can be expressed simply as

$$\left(\frac{\partial F}{\partial x}\right)^{(\ell)}_{m,n} = \frac{1}{\Delta x}\left\{F^{(\ell)}_{m,n} - F^{(\ell-1)}_{m,n}\right\}, \tag{4.1}$$

where Δx is the increment in x:

$$\Delta x = x^{(\ell)}_{m,n} - x^{(\ell-1)}_{m,n}. \tag{4.2}$$

The cross-plane: ℓ, does not in general correspond to a plane of constant x, and so the first-order backward-difference approximation to $\partial F/\partial z$ has to be written

$$\left(\frac{\partial F}{\partial z}\right)^{(\ell)}_{m,n} = \frac{1}{\Delta z^-}\left\{(1-\lambda^-)F^{(\ell)}_{m,n} + \lambda^- F^{(\ell-1)}_{m,n} - F^{(\ell)}_{m,n-1}\right\}, \tag{4.3}$$

where

$$\lambda^- = \frac{1}{\Delta x}\left\{x^{(\ell)}_{m,n} - x^{(\ell)}_{m,n-1}\right\}, \tag{4.4}$$

and

$$\Delta z^- = z^{(\ell)}_{m,n} - z^{(\ell)}_{m,n-1}. \tag{4.5}$$

Correspondingly, the first-order forward-difference approximation to $\partial F/\partial z$ is written

$$\left(\frac{\partial F}{\partial z}\right)^{(\ell)}_{m,n} = \frac{1}{\Delta z^+}\left\{F^{(\ell)}_{m,n+1} + (1 - \lambda^+)F^{(\ell)}_{m,n} - \lambda^+ F^{(\ell-1)}_{m,n}\right\}, \qquad (4.6)$$

where
$$\lambda^+ = \frac{1}{\Delta x}\left\{x^{(\ell)}_{m,n} - x^{(\ell)}_{m,n+1}\right\}, \qquad (4.7)$$

and
$$\Delta z^+ = z^{(\ell)}_{m,n+1} - z^{(\ell)}_{m,n}. \qquad (4.8)$$

In Equation (2.32), $\partial F/\partial z$ is approximated by a backward, or forward, difference according to the sign of A_3: backward if $A_3 > 0$ and forward if $A_3 < 0$. Thus the derivative is always formed in the upwind direction, so as to preserve convective stability. Elsewhere, the arithmetic mean of the backward and forward difference is taken; it will be noted that this procedure is not necessarily equivalent to a central difference because Δz^- is not necessarily equal to Δz^+.

In order to express the first derivative with respect to y, in difference form, it is convenient to write the term $A_4 \partial F/\partial y$, in Equation (2.32) as

$$A_4 \frac{\partial F}{\partial y} = \left[A_4^{(1)} + A_4^{(2)}\right] \frac{\partial F}{\partial y}, \qquad (4.9)$$

where $A_4^{(1)}$ contains only diagonal elements and $A_4^{(2)}$ only off-diagonal elements. Then:

$$A_4\left(\frac{\partial F}{\partial y}\right)^{(\ell)}_{m,n} = \frac{A_4^{(1)}}{2}\left[(\phi + I)F^{(\ell)}_{m+1,n} - 2\phi F^{(\ell)}_{m,n}\right.$$

$$\left. + (\phi - I)F^{(\ell)}_{m-1,n}\right] + \frac{A_4^{(2)}}{2}\left[F^{(\ell)}_{m+1,n} - F^{(\ell)}_{m-1,n}\right]. \qquad (4.10)$$

The quantity Φ, in Equation (4.10) is a diagonal matrix, equivalent to the parameter α employed in Reference [16], which controls the level of artificial viscosity to be introduced via the difference equations. The elements of Φ: ϕ_i, lie between -1 and 1, and have the same sign as the corresponding terms of $A_4^{(1)}$. The difference equations become unconditionally stable if $|\phi_i| = 1$, but are only conditionally stable if $|\phi_i| < 1$. It will be noted that no artificial viscosity is introduced via the off-diagonal terms of A_4; this is appropriate since any artificial viscosity so introduced would relate one element of $\partial F/\partial x$ to another element of $\partial^2 F/\partial y^2$, with unpredictable results.

Second derivatives with respect to y are expressed in the usual form

$$\left(\frac{\partial^2 F}{\partial y^2}\right)^{(\ell)}_{m,n} = \frac{1}{(\Delta y)^2}\{F^{(\ell)}_{m+1,n} - 2F^{(\ell)}_{m,n} + F^{(\ell)}_{m-1,n}\}, \quad (4.11)$$

where

$$\Delta y = y^{(\ell)}_{m+1,n} - y^{(\ell)}_{m,n} = y^{(\ell)}_{m,n} - y^{(\ell)}_{m-1,n}. \quad (4.12)$$

Upon introduction of the various difference approximations into Equation (2.32), the following difference equation is obtained, relating to the node point ℓ, m, n (see Figure 9):

$$B_1 F^{(\ell)}_{m+1,n} + B_2 F^{(\ell)}_{m,n+1} + B_3 F^{(\ell)}_{m,n}$$

$$+ B_4 F^{(\ell)}_{m-1,n} + B_5 F^{(\ell)}_{m,n-1} = B_6 F^{(\ell-1)}_{m,n}, \quad (4.13)$$

where the B's are square matrices representing linear combinations of the A's in Equation (2.32).

3. ALTERNATING-DIRECTION SCHEME

The forward-marching procedure advances in the positive x-direction, from a cross-plane: $\ell-1$, where the solution is assumed to be known, to a cross-plane: ℓ, at which a new solution is sought. The cross-plane is scanned alternately in the n-, and m-directions (Figures 10, 11), converting Equation (4.13), respectively, into the successive forms:

$$B_1 F^{(\ell)}_{m+1,n} + B_3 F^{(\ell)}_{m,n} + B_4 F^{(\ell)}_{m-1,n} = C_1 \ , \tag{4.14}$$

$$B_2 F^{(\ell)}_{m,n+1} + B_3 F^{(\ell)}_{m,n} + B_5 F^{(\ell)}_{m,n-1} = C_2 \ . \tag{4.15}$$

in which C_1, C_2 contain the passive terms originating on the left-hand side of Equation (4.13). During the scan in the n-direction, Equation (4.14) represents a recursion relationship for $1 \leq m \leq M$, and, during the scan in the m-direction, Equation (4.15) represents one for $1 \leq n \leq N$. In either case the sequence of Equations (4.14, 15) may be written in the form

$$PQ = R \ , \tag{4.16}$$

where Q is a vector of order M or N, whose elements are the vectors F, R is a vector of similar order containing the elements C_1 or C_2, and P is a tridiagonal square matrix, of order M or N, containing the B's from Equation (4.14) or (4.15).

During any given iteration P and R are regarded as known, and the solution of Equation (4.16) is formally determined as

$$Q = P^{-1} R \, . \tag{4.17}$$

The solution is readily calculated using the extended Choleski method (Reference [17]) which involves forward elimination of the lower diagonal elements of P, and backward substitution to determine the elements of Q. The coefficient matrices P, R are updated in successive iterations and the solution process continued until convergence is obtained.

SECTION V

ADDITIONAL DETAILS OF THE METHOD

1. EXTERNAL FLOW

It is assumed that the external flow conditions are specified in terms of the local pressure coefficient, C_p, together with conditions in the undisturbed free stream. The local static pressure, static temperature, Mach number, and resultant velocity in the external flow can be determined, directly, as follows:

$$\frac{p}{p_\infty} = 1 + \gamma \frac{M_\infty^2}{2} C_p \,, \tag{5.1}$$

$$\frac{T_e}{T} = \left(\frac{p}{p_\infty}\right)^{\frac{\gamma-1}{\gamma}} \tag{5.2}$$

$$M_e^2 = \frac{2}{\gamma-1} \left\{ \left(1 + \frac{\gamma-1}{2} M_\infty^2\right) \frac{T_\infty}{T_e} - 1 \right\} \tag{5.3}$$

$$\frac{Q_e}{Q_\infty} = \frac{M_e}{M_\infty} \frac{T_e}{T_\infty}^{1/2} \tag{5.4}$$

The velocity components, U_e, W_e, cannot be determined directly, but must be found by solving the Euler equations (the momentum equations without the viscous and turbulent shear-stress terms) subject to the appropriate boundary conditions. These equations are solved implicitly, in the two-dimensional domain: x, z, using the same difference approximations as are employed for the full boundary-layer equations.

Truncation errors associated with these difference approximations will of course, arise and, as a result, the values of U_e and W_e derived will not generally be consistent with the value of Q_e determined from Equation (5.4). The truncation errors can however, be reduced for

certain types of flow, by suitable handling of the pressure gradients: $\partial p/\partial x$, $\partial p/\partial z$. In particular, for an infinite yawed wing, a transformation of the form:

$$C_{p_T}^2 = \cos^2\Lambda - \frac{2}{(\gamma-1)M_\infty^2}\left\{\left(1 + \frac{\gamma M_\infty^2}{2} C_p\right)^{\frac{\gamma-1}{\gamma}} - 1\right\}, \quad (5.5)$$

will enable the exact values of U_e, W_e, to be obtained using a two-point backward difference for $\partial C_p/\partial x$:

$$\frac{\partial C_p}{\partial x} = \frac{2}{\Delta x}\left\{\left(1 + \frac{\gamma M_\infty^2}{2} C_p\right)^{1/\gamma}\right\}_n^{(\ell)} \left\{(C_{p_T})_n^{(\ell)} - (C_{p_T})_n^{(\ell-1)}\right\} \quad (5.6)$$

and a three-point difference for $\partial C_p/\partial z$:

$$\frac{\partial C_p}{\partial z} = \left\{\left(1 + \frac{\gamma M_\infty^2}{2} C_p\right)^{1/\gamma}\right\}_n^{(\ell)} \left\{\frac{1}{\Delta z^+}(C_{p_T})_{n+1}^{(\ell)} - \left(\frac{1-\lambda^+}{\Delta z^+}\right.\right.$$

$$\left.\left. - \frac{1-\lambda^-}{\Delta z^-}\right)(C_{p_T})_n^{(\ell)} - \left(\frac{\lambda^+}{\Delta z^+} - \frac{\lambda^-}{\Delta z^-}\right)(C_{p_T})_n^{(\ell-1)} - \frac{1}{\Delta z^-}(C_{p_T})_{n-1}^{(\ell)}\right\} \quad (5.7)$$

The transformed pressure coefficient: C_{p_T}, will be recognized as being identical to the velocity component normal to the sweep lines, and the quantity

$$\left(1 + \frac{\gamma M_\infty^2}{2} C_p\right)^{1/\gamma},$$

in Equations (5.6,7) as being identical to the local density ratio: ρ_e/ρ_∞.

In the present formulation, the above transformation is used for the finite swept wing also. In this more general case truncation errors will arise in the solution of the Euler equations but, in most cases, they will be smaller than the errors that would arise if $\partial C_p/\partial x$, $\partial C_p/\partial z$ were determined by applying the difference formulae to the untransformed pressure coefficients. It should be stressed however, that no approximation is introduced into the Euler equations other than the difference approximations to the derivatives.

2. DISTRIBUTION OF NODE POINTS THROUGH THE BOUNDARY LAYER

The thickness of the integration domain is set equal to $\Omega\delta$, where δ is the boundary layer thickness and Ω is a constant in the neighborhood of 1.25. Thus, if the physical distance from the wall is denoted by $\hat{y}$, then

$$0 \leq \hat{y} \leq \Omega\delta \quad \text{as} \quad 0 \leq m \leq M ,$$

where M is the number of node points distributed through the domain. The transformed space variable, y, is defined by

$$y = m\Delta y , \tag{5.8}$$

where Δy is any convenient constant, and hence the relationship between y and $\hat{y}$ describes the manner in which the node points are distributed.

For laminar flow, a uniform distribution is appropriate, whereupon

$$\hat{y} = \Omega\delta m/M , \tag{5.9}$$

$$h_2 = \partial\hat{y}/\partial m = \Omega\delta/M , \tag{5.10}$$

$$K_{22} = 0. \tag{5.11}$$

For turbulent flow, a non-uniform distribution is more appropriate which provides increased point-density in the region of large gradients close to the wall. A distribution that respects the various regions of a turbulent boundary layer: viscous sublayer, logarithmic region, and "wake region" is

$$\hat{y} = \frac{\phi\delta}{(1 + \phi)M} \{c_1(m-M) + \Omega M\} , \tag{5.12}$$

in which $\phi = \phi(m)$ is such that ϕ becomes large as $m \to M$. The distribution thus reduces to the uniform one

$$\hat{y} = \frac{\delta}{M} \{c_1(m-M) + \Omega M\} , \tag{5.13}$$

in the outer part of the boundary layer. In the inner part, the distribution is controlled by the function ϕ which takes the form

$$\phi = c_2 m + c_3(e^{c_4 m} - 1) . \tag{5.14}$$

Here, c_3 is taken to be proportional to the additive constant in the Law of the Wall, and c_2 determines the distance from the wall at which it is desired to place the first node point; c_4 is selected such that y is non-singular in the interval $0 \leq m \leq M$.

The values of h_2 and K_{22}, corresponding to Equation (5.12) can be determined by differentiation with respect to m:

$$h_2 = \frac{\delta}{M} \frac{c_1\delta}{1 + \phi} + \frac{[c_1(m-M) + \Omega M]}{(1 + \phi)^2} \phi' \tag{5.15}$$

$$h_2^2 K_{22} = \frac{\delta}{M} \frac{2c_1\phi'}{(1+\phi)^2} + [c_1(m-M) + \Omega M]$$

$$\cdot \frac{\phi''}{(1+\phi)^2} - \frac{2\phi'^2}{(1+\phi)^3} \quad . \qquad (5.16)$$

SECTION VI

EVALUATION OF THE METHOD

Time and funding constraints have placed severe limitations on the scope of the validation procedures which could be performed on the method. The following represent only a cursory set of checks to determine whether gross errors were likely to arise when the method was used. A more comprehensive process of validation is clearly needed, to search for more subtle errors or inaccuracies, involving checks of internal consistency as well as comparisons with experiment and exact theory. These comparisons would also form a basis for "fine tuning" of the method (adjustment of the empirical functions, etc.) which, so far has not been done.

A number of numerical convergence checks were made using, as a simple test case, two-dimensional, incompressible laminar flow over a flat plate. Figure 12 shows the effect of varying the number of node points distributed through the boundary layer. It is evident that 20 points is sufficient to adequately recover the exact Blasius solution and that further refinement has no significant effect. The results shown were obtained using 7 streamwise stations (including the leading edge which was represented as a stagnation point from which the fluid accelerated linearly to free-stream velocity in a distance equal to 0.005 times the length of the plate). A coarser description involving only 5 streamwise stations resulted in a 4% error in wall velocity gradient compared to an error of less than 1% with 7 stations. A finer description, involving 14 streamwise stations, reduced this error to less than 0.05%.

Figure 13a shows the convergence of the iteration process for the case involving 7 streamwise stations and 20 node points across the

boundary layer. At this particular x-station (the 7^{th}) the calculation converged to a tolerance of 10^{-4} in 6 iterations. Here, the tolerance is defined as the maximum permissible variation between successive iterations, expressed as a fraction of U_e. (Corresponding tolerances are placed, where applicable, on W, T, and $\overline{q^2}$). Relaxation of the tolerance results in progressively larger errors in wall velocity gradient (Figure 13b); with a tolerance of 0.003 this error is about 8%.

Figure 14a shows the predicted effect of compressibility on the two-dimensional laminar boundary layer. The calculations indicate a reduction of about 16% in normalized wall shear stress at a Mach number of 3. This order of reduction is close to the figure given by Young's formula [18]. Figure 14b shows the computed temperature profile through the laminar boundary layer at Mach numbers of 2 and 3. The profiles show the enthalpy is being properly conserved in the outer part of the boundary layer. The loss of enthalpy near the wall is of course to be expected because the recovery factor is less than one.

Figure 15 shows some calculated results for incompressible laminar flow over an infinite 45°-swept wedge. The external velocity component: U_{e_n}, normal to the leading edge, is assumed to increase in proportion to the normal distance: x_n, while the external component: W_{e_p}, parallel to the leading edge is constant. The computed velocity profiles are expressed in similarity form and are compared with the exact solution of Howarth and Cooke [19,20]. It should be noted that the calculation proceeded, not along the normal to the leading edge, but in the direction of the undisturbed stream. The velocity profiles: U(y), W(y), appearing in the calculation did not, therefore, reach an asymptotic form

but varied with x. The profiles plotted in Figure 15 were obtained by resolution.

Some results for incompressible turbulent flow are presented in Figures 16 through 19. Figure 16 shows an inner-law plot of the velocity profiles in a constant-pressure turbulent boundary layer at 4 Reynolds numbers. It will be noted that the viscous sublayer and blending region are well represented, and that the familiar logarithmic region is obtained at high Reynolds numbers. The slope of the logarithmic portion is consistent with the value of von Karman's constant used here (0.418); the additive constant emerges as 2.5, compared with Patel's [4] value of 2.3.

The predicted wall shear stress is expressed as a function of Reynolds number in Figure 17. The trend is consistent with that given by Rotta [21], Coles [22], and Smith and Walker [23], although the predicted values themselves appear to be slightly low.

Figure 18 shows the computed mean velocity profile at a Reynolds number (R_{δ^*}) of 10^4. Two sets of results are plotted, corresponding to 20 and 30 node points across the boundary layer, and there is no significant difference between them. The calculations are in good agreement with the experimental data of Klebanoff [24] and Smith and Walker [23]. The corresponding profiles of turbulence intensity: $\overline{q^2}$, are shown in Figure 19. It will be noted that $\overline{q^2}$ increases from zero, at the wall, to a maximum (for constant - pressure flow) which is located near the edge of the viscous sublayer. The maximum value: $\overline{q^2}/U_e^2 = 0.0085$, is consistent with the predicted wall shear stress of 0.0013, assuming a value of a_1 ($=-\overline{uv}/\overline{q^2}$) equal to 0.15. The calculated results are compared with the data of

Klebanoff [24]. Experimental values of $\overline{q^2}$ are shown and also the measured values of $-\overline{uv}$ divided, here, by a_1. The two sets of experimental data are in close agreement with each other over most of the boundary layer, but diverge close to the wall because of the "inactive" component of the turbulence included in $\overline{q^2}$. The calculated results are in closer agreement with the values of $-\overline{uv}/a_1$, in this region, confirming that the quantity $\overline{q^2}$ considered in the theory is to be identified with the active component of the turbulence which is responsible for momentum transport.

SECTION VII

DEMONSTRATION TEST CASE

The test case selected for demonstration purposes corresponds to the upper surface of the right wing of the NASA/Air Force TACT (modified F 111) airplane. The wing geometry and flight pressure distributions have been supplied by NASA Flight Research Center, Edwards, California. The particular case, for which a boundary layer calculation has been performed corresponds to a nominal leading edge sweep angle of 26°, and an airplane angle of attack of 9.01°. The Mach number is 0.84, and the static pressure is 903.08 lb/ft^2.

The wing geometry is shown in Figure 20. The pressures were measured, in flight, along four spanwise stations designated Rows A through D, in which Row A is near the tip, and Row D near the junction with the inner-wing glove. The instrumented portion of the wing was clean, and was uniformly tapered. The pressure distributions, along the four spanwise stations are shown in Figure 21, and it will be noted that a shock is present over most of the span. The shock appears to be simple at Rows B and C, but becomes bifurcated at Row A, near the wing tip.

The calculation was performed with 15 streamwise stations and four spanwise stations (corresponding to Rows D, B, C, A). The end stations (D,A) were treated as being portions of locally-infinite-swept wings. In the interior of the integration domain (Rows C,B) the flow was treated as being fully three-dimensional. Transition was assumed to occur at 11% of local streamwise chord, on Rows D, C, and at 6% of local chord on Rows B,A. These stations correspond to the start of the adverse streamwise pressure gradient.

Figures 22 and 23 present the distributions of δ^*, τ_{w_x}, and τ_{w_z} versus local chord at the four spanwise stations. Figure 24 presents velocity profiles as computed at three representative points on the planform. Separation occurred in a small region, depicted approximately in Figure 24, and the separation control process was used to recover the boundary layer calculation. Evidence of approaching separation can be seen in Figures 22 and 23 through the behavior of δ^* and τ_{w_x}.

SECTION VIII
CONCLUSIONS AND RECOMMENDATIONS

The method described herein builds upon experience in calculating three-dimensional boundary layers extending over some eight years. This experience has been reflected in the retention of many of the more firmly-based features of the earlier methods, and these features have been incorporated, together with many new ones, into an entirely new program structure. The new structure offers immediate computational advantages with respect to the ease of setting up a calculation and the economy of the calculation itself. It also offers considerable flexibility which will permit extensions and refinements of the method as the need for them arises. In that regard the method may be considered to be a starting point for further work, rather than a completed product, even though it offers the user a comprehensive tool which should more than adequately perform the tasks for which it is currently needed. It will clearly take time to properly evaluate the new method, and to exploit its full potential.

Central to the new program structure is the alternating-direction implicit (ADI) numerical scheme. We believe that the adoption of this type of numerical scheme represents a definitive solution of several of the problems which have plagued the development of implicit methods for calculating three-dimensional boundary layers. We also believe that it represents the best starting point for several potential extensions of the method, involving, for instance, the inclusion of higher-order terms in the equations of the mean motion and/or the turbulence model equations.

A number of further refinements to the numerical scheme would, however, be worthwhile even for flows which satisfy the first-order

boundary-layer equations. In particular, it would be advantageous to upgrade the scheme to second-order accuracy with respect to the x- and z-derivatives. Also, improvements could be made to accelerate the convergence of the iteration process. Schemes which claim to eliminate the need for the iteration process, altogether, should be evaluated too; but the present authors are skeptical about the desirability of such schemes if they place severe restrictions on the step-size in the direction of march. If this is, indeed, the case, the iteration process has simply been traded for a much larger number of x-steps.

One of the features of the earlier methods, which has been retained, is the one-equation turbulence model. We have consistently argued the superiority of such a model, over the "zero-equation" eddy-viscosity or mixing-length approaches, on the grounds of its greater universality. On the other hand, this universality could be improved still further by the incorporation of at least one more differential equation: for the dissipation rate or, equivalently, the turbulence length scale. We recommend that this refinement be made, possibly in an experimental method, to enable the user to check the validity of the existing model under specified flow conditions where its adequacy might be questionable.

To the extent that the turbulence model is closely similar to that used in the earlier methods, it would be expected that the degree of correlation between the predicted mean-flow quantities and experiment, would be comparable to that previously reported for turbulent flow [1,3,4]. A wider range of measurements is now available, however, and it would seem highly desirable to make comparisons with these recently acquired data.

The comparisons would serve as a further check on the reliability of the method, and might also indicate the areas where "fine-tuning" of the empirical functions would produce even better agreement with experiment. It is worth noting that the assumed relationship between dissipation length and position through the boundary layer, and the diffusion function assumed herein, are identical to their counterparts in the earlier method [3,4].

Some improvements can still be made to the geometry-representation scheme. The conical-projection approach is probably adequate for most purposes, but it could be upgraded to a full doubly-curved representation, with correspondingly greater generality, without difficulty. The governing equations are already cast in terms of two geodesic curvatures. In this regard, however, we feel that there is a need to accumulate user experience in the description of typical airplane geometries, prior to the decision to replace the existing scheme.

One of the major sources of uncertainty, concerning a boundary-layer calculation extending only over the wings of an airplane configuration, has to do with the specification of realistic boundary conditions at the wing root. Fluid spilling off the fuselage, onto the wing, convects information which is relevant to the boundary-layer development but which the user is unable to specify. Ideally, the calculation should extend over the whole of the wetted surface of the airplane, in which case the need for specifying boundary conditions along such arbitrary interfaces would be eliminated. Unfortunately, such interfaces often correspond, as does the wing-fuselage junction, to regions where the first-order boundary-layer equations are invalid, and where a more sophisticated

calculation would be required. Be that as it may, the present method could readily be extended to a wing-fuselage combination on the assumption that the corner flow is amenable to first-order treatment. The extended method would, at least, take account of continuity of mass across the interface, and would partially represent the momentum exchange too. We strongly recommend that such an extension of the method be funded, at an early date, to provide an interim engineering tool for airplane boundary-layer computations, and to provide a framework for incorporation of the more sophisticated treatment of the corner flow when the technology for handling it becomes available.

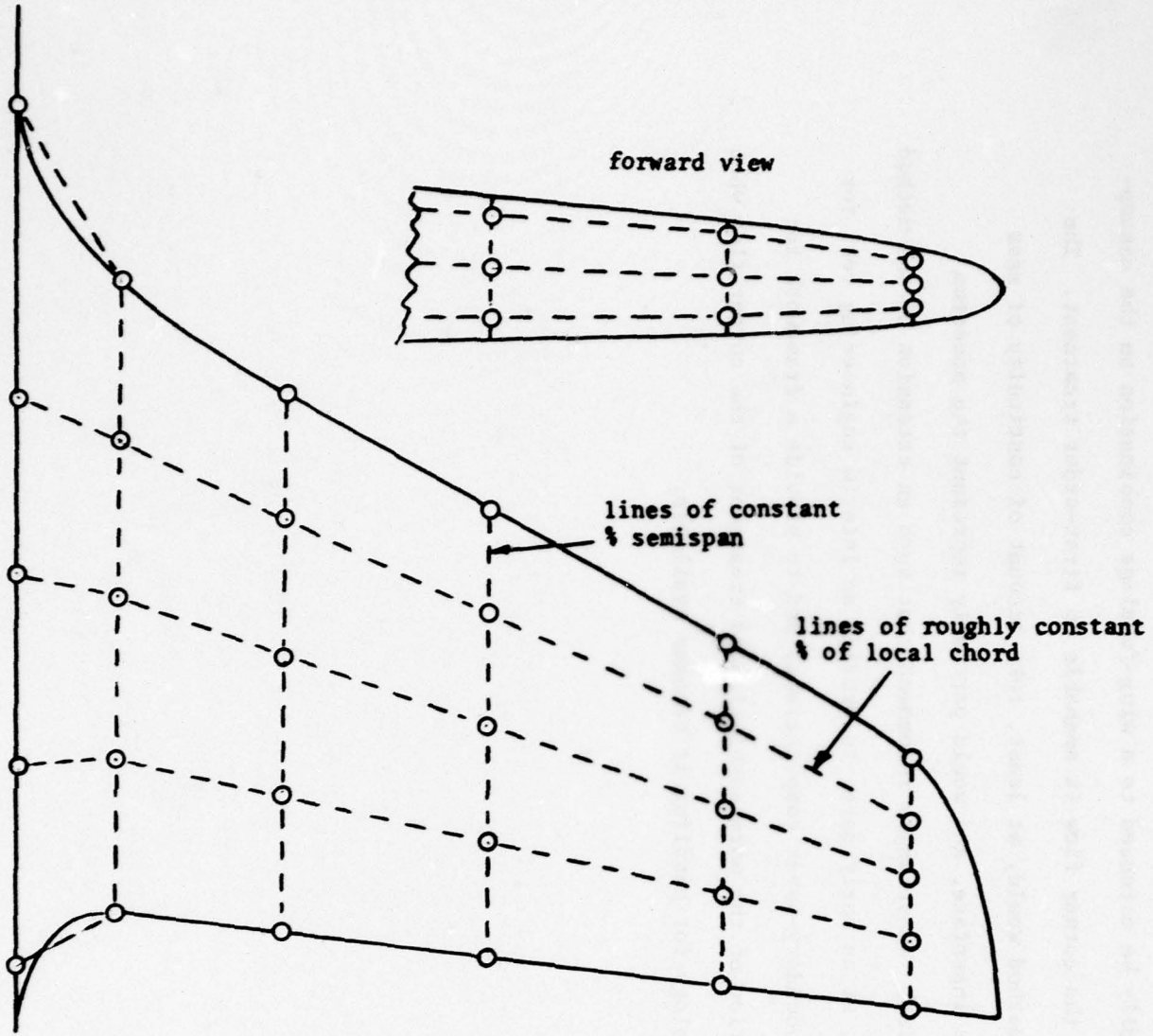

Figure 1 WING GEOMETRY, SHOWING SEGMENTATION INTO PANEL ELEMENTS

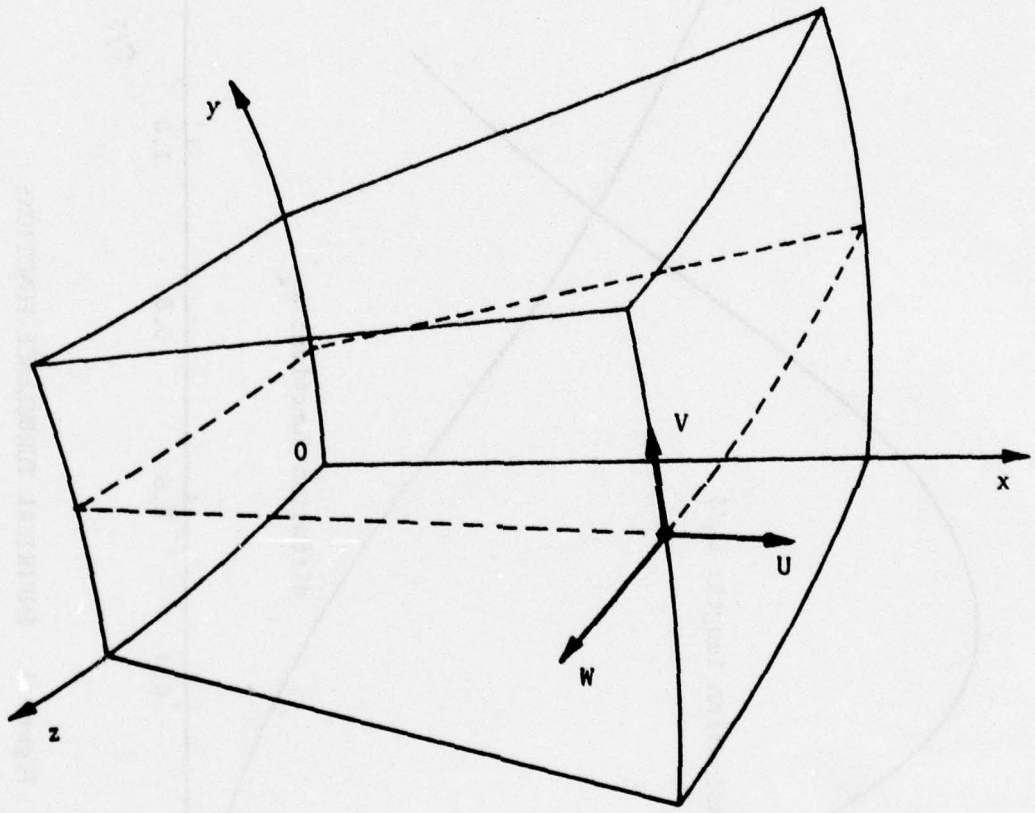

Figure 2 LOCAL ORTHOGONAL COORDINATE SYSTEM

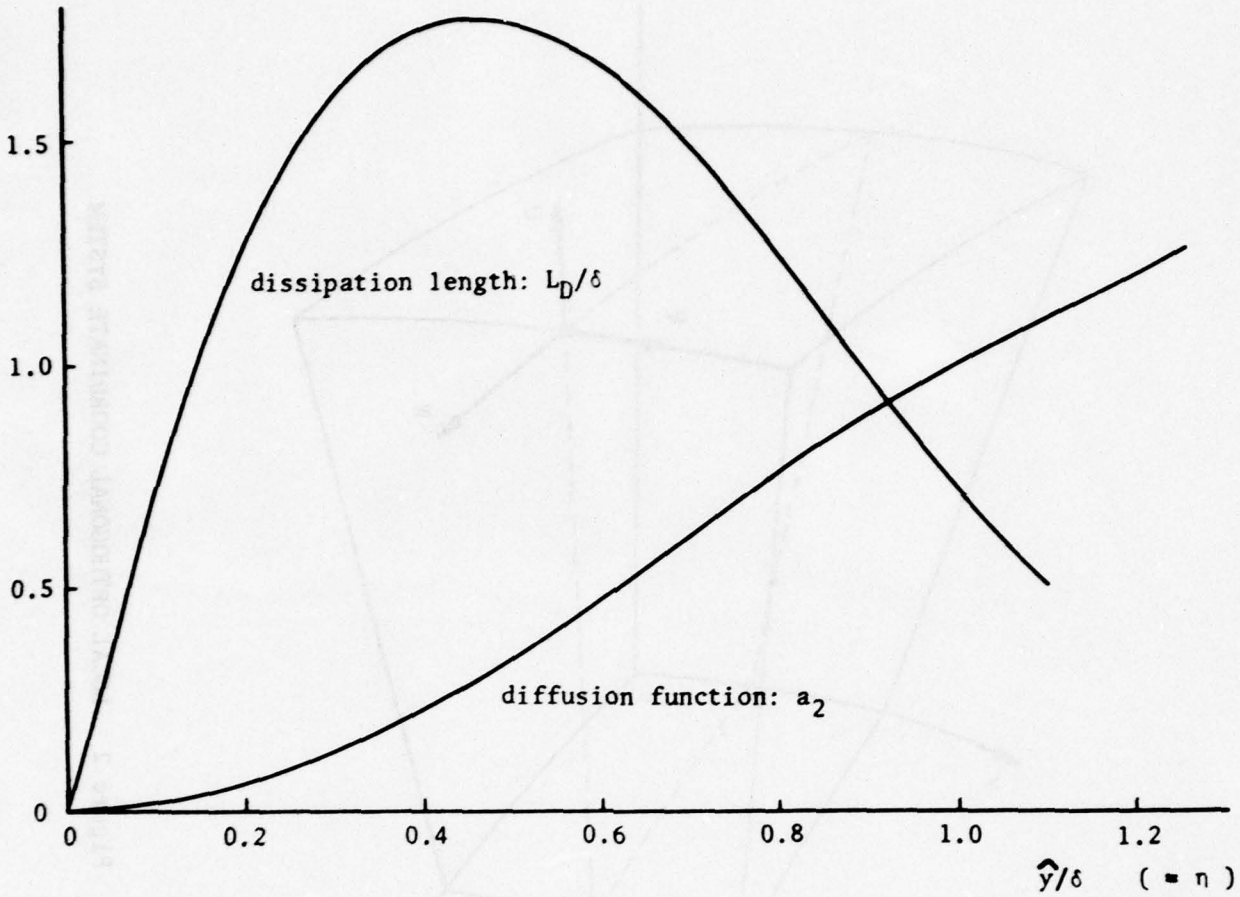

Figure 3 EMPIRICAL TURBULENCE FUNCTIONS

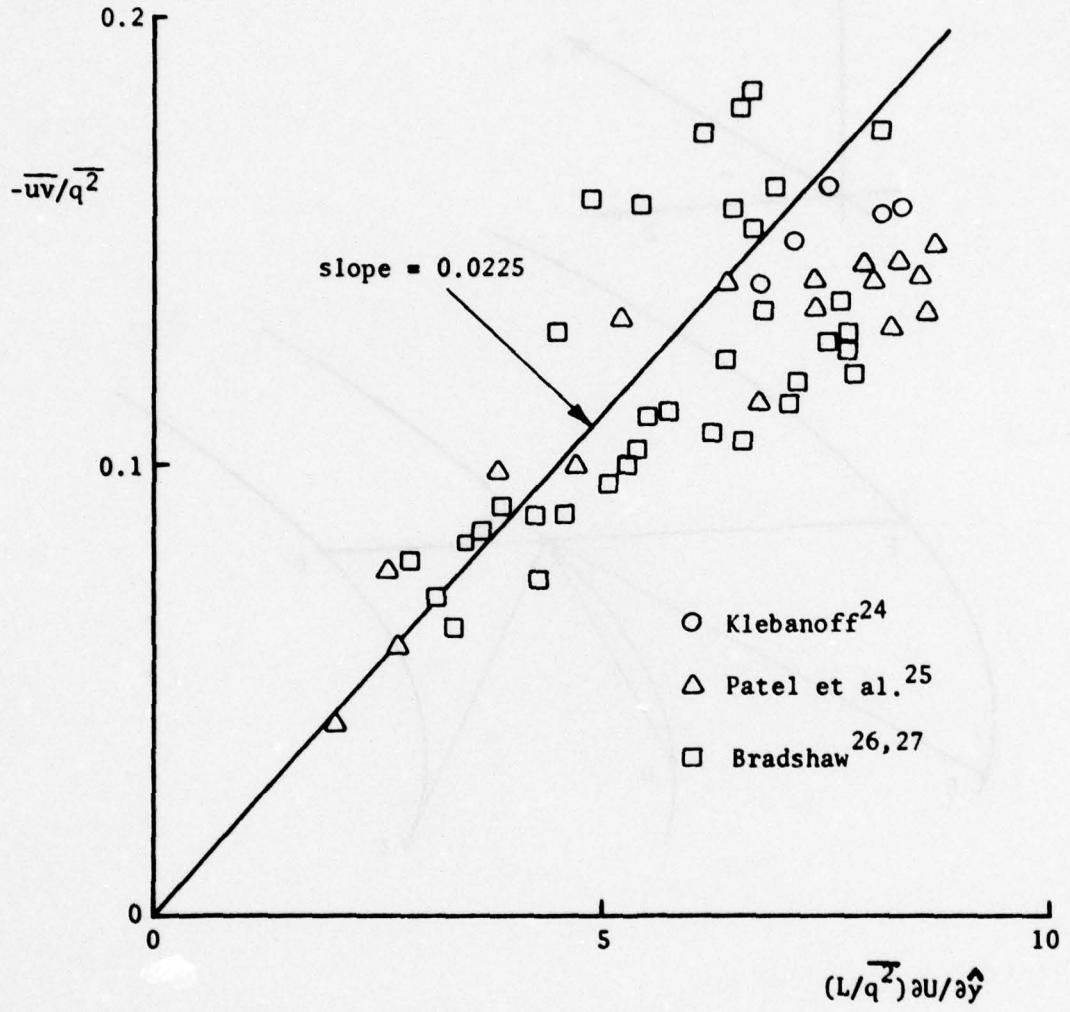

Figure 4 EMPIRICAL RELATIONSHIP BETWEEN SHEAR STRESS AND TURBULENT KINETIC ENERGY

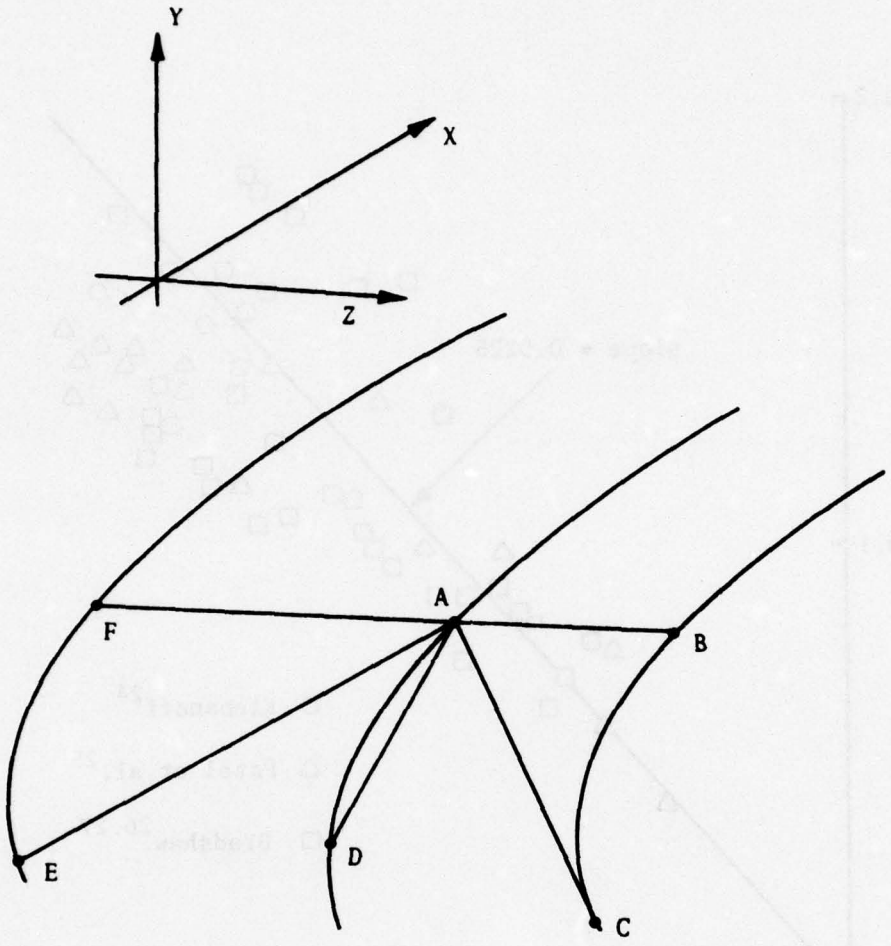

Figure 5 LOCAL SURFACE DEVELOPMENT

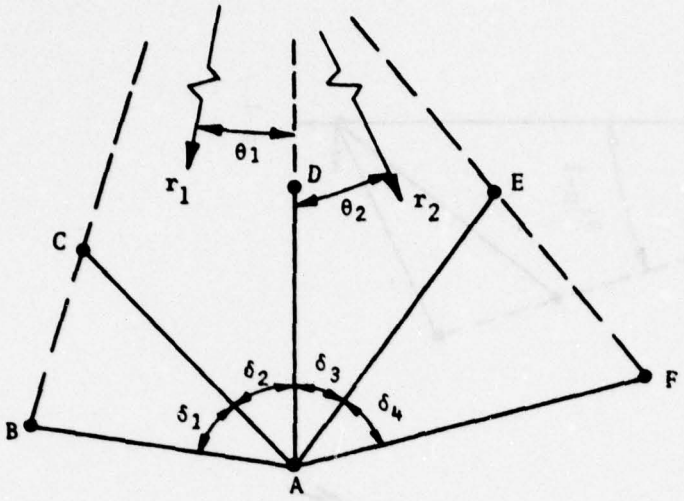

Figure 6(a) CONICAL DEVELOPMENT ABOUT POINT A

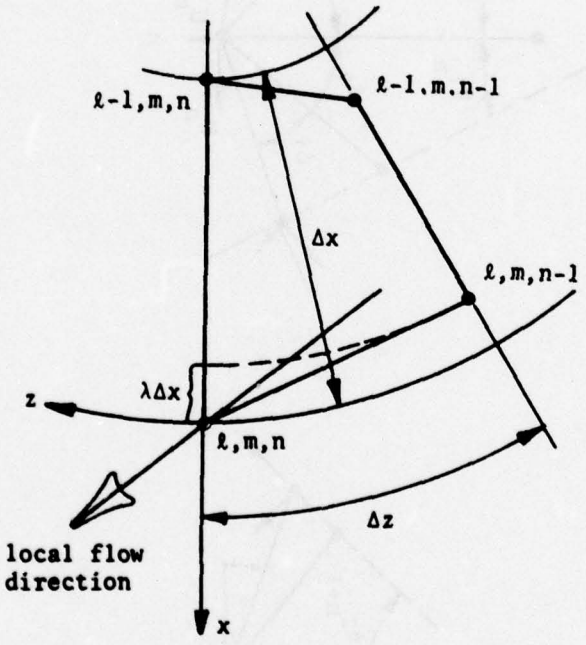

Figure 6(b) FINITE DIFFERENCING FOR NON-RECTANGULAR ELEMENT

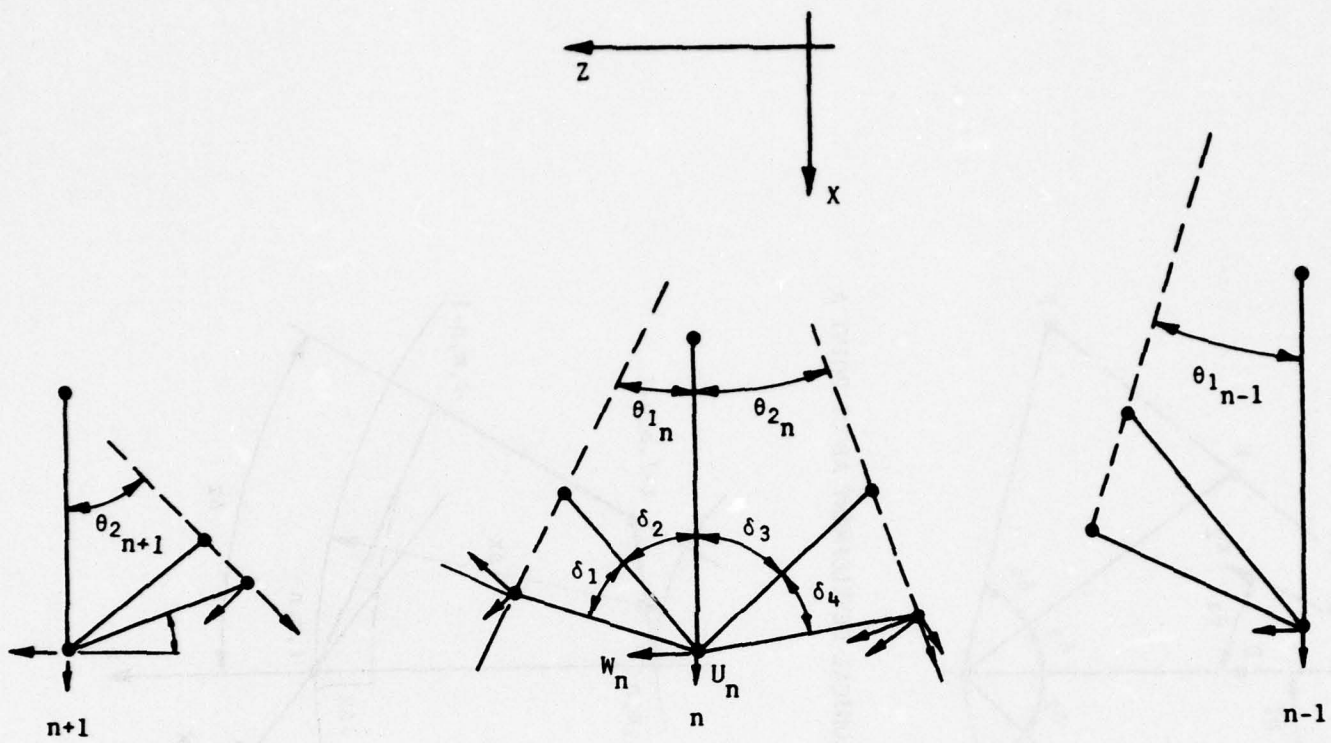

Figure 7 LATERAL ROTATIONS BETWEEN ADJACENT ELEMENTS OF THE SAME ROW

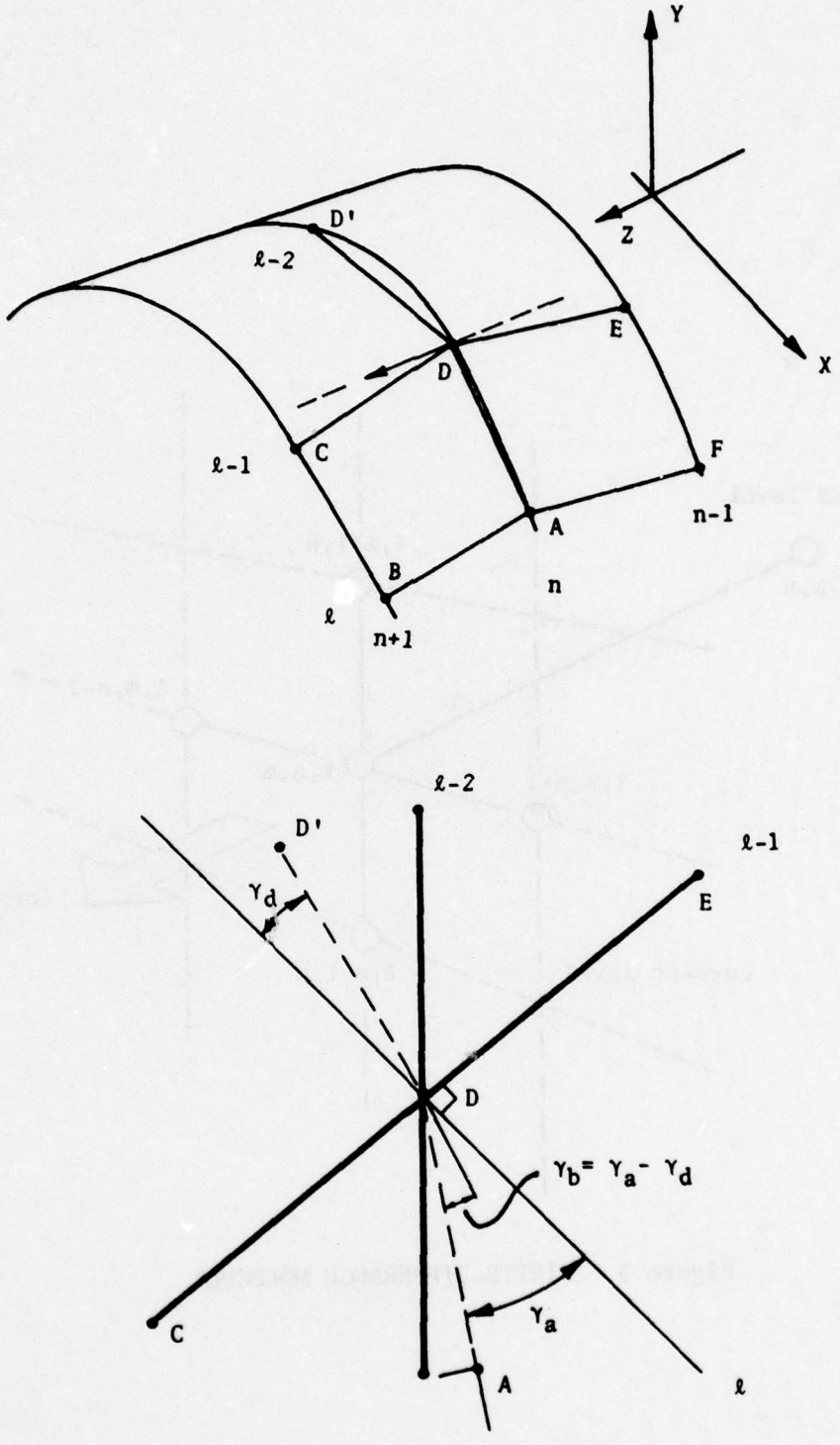

Figure 8 BACKWARD ROTATIONS BETWEEN ADJACENT ELEMENT ROWS

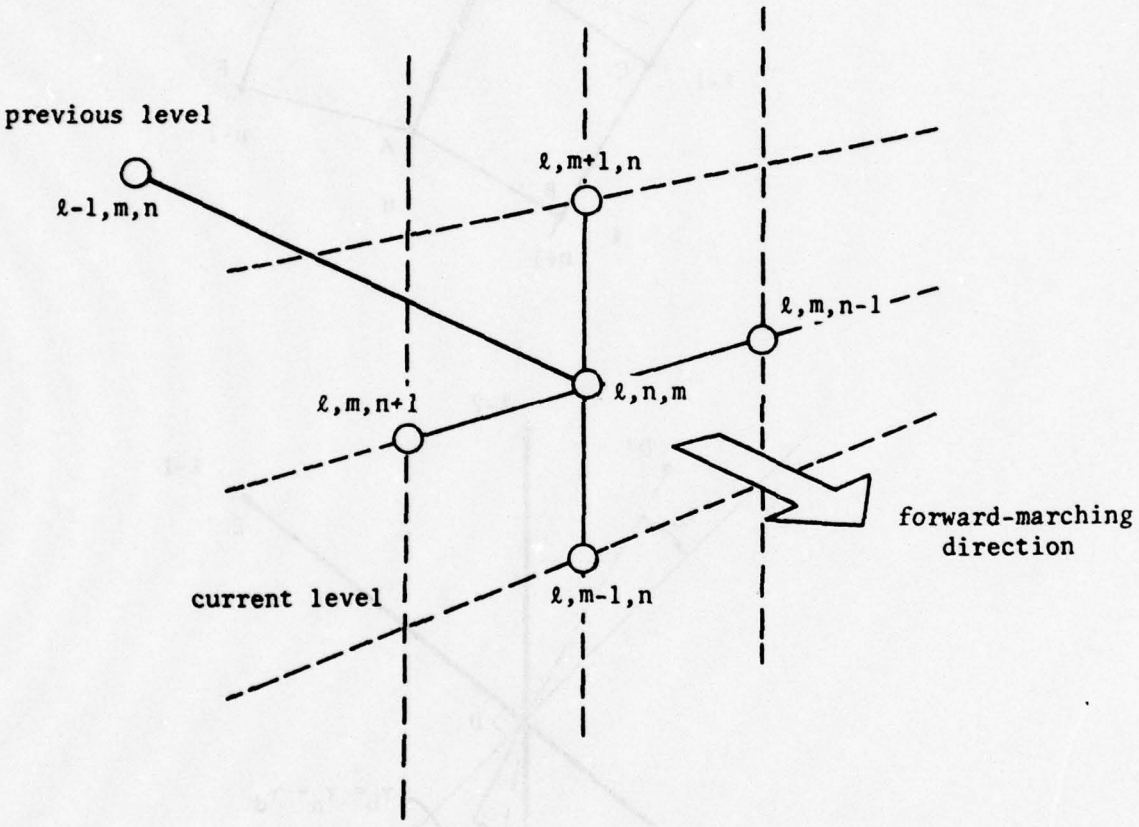

Figure 9 FINITE-DIFFERENCE MOLECULE

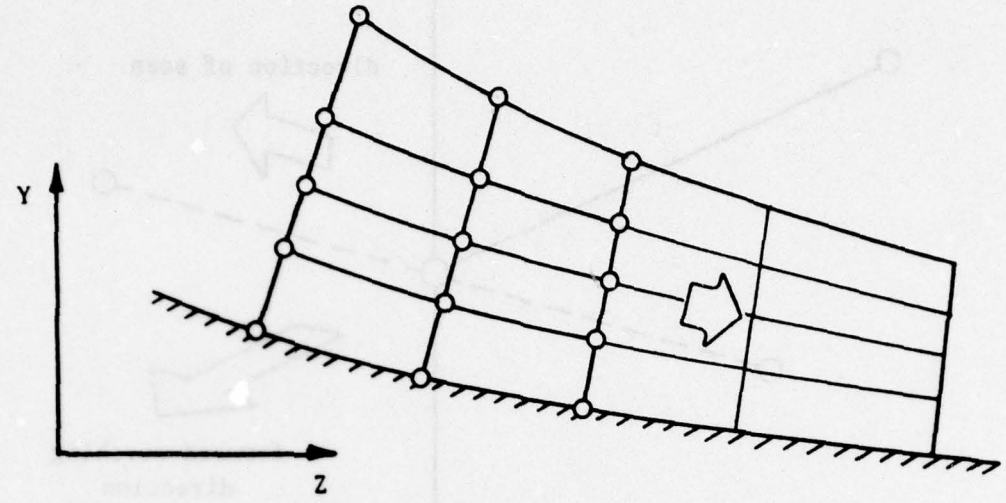

(a) Horizontal Scan

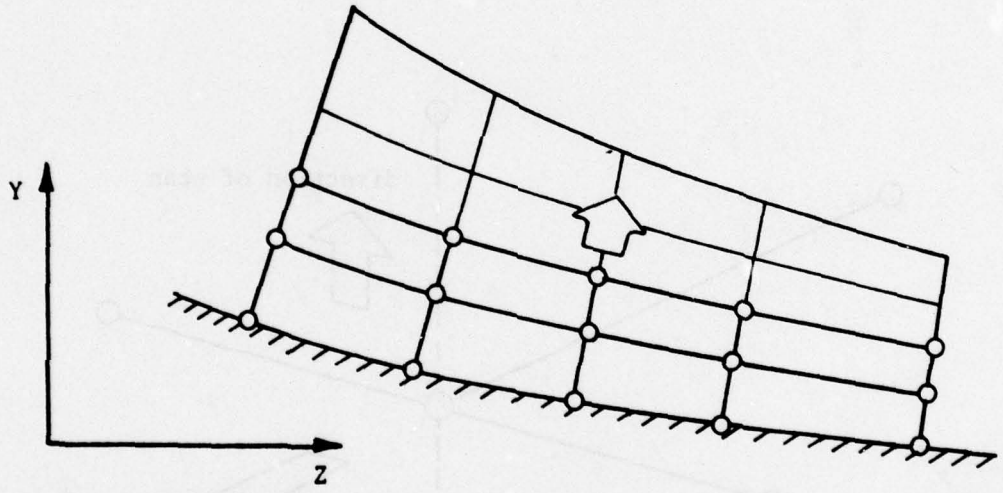

(b) Vertical Scan

Figure 10 ALTERNATING-DIRECTION SCHEME

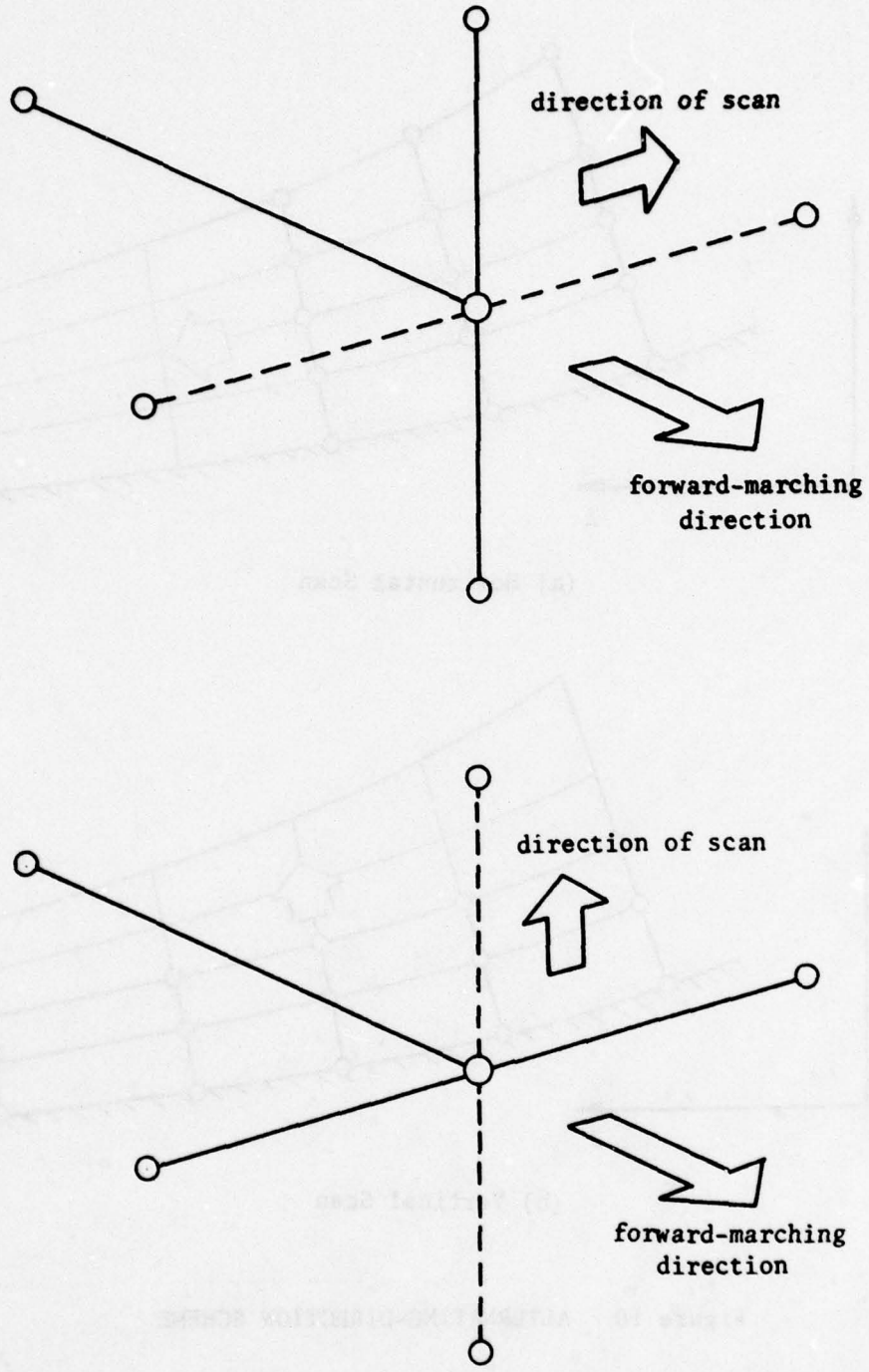

Figure 11 FINITE-DIFFERENCE MOLECULE, SHOWING ALTERNATING-DIRECTION SCANNING

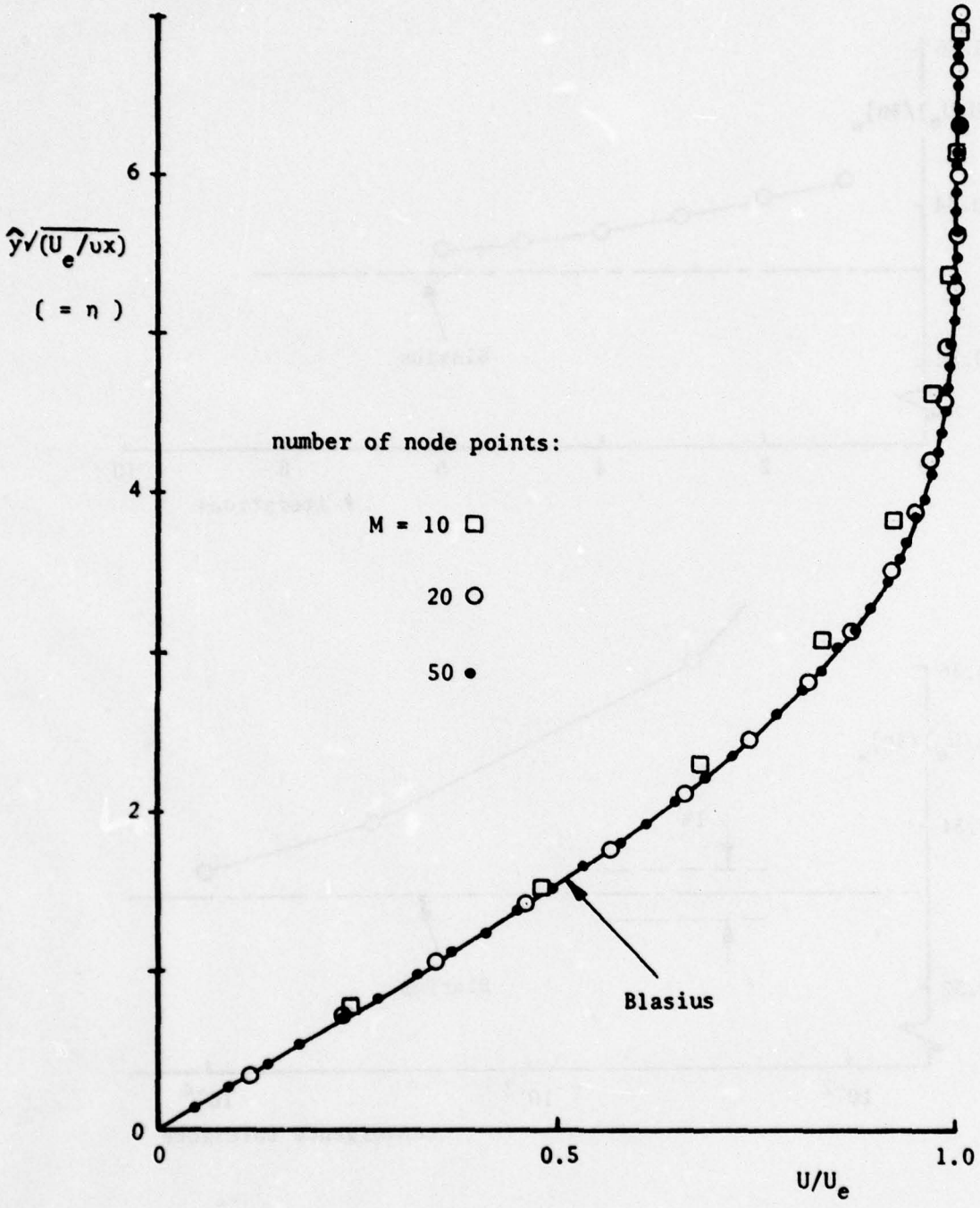

Figure 12 TWO-DIMENSIONAL, INCOMPRESSIBLE LAMINAR FLOW OVER A FLAT PLATE: VELOCITY PROFILES

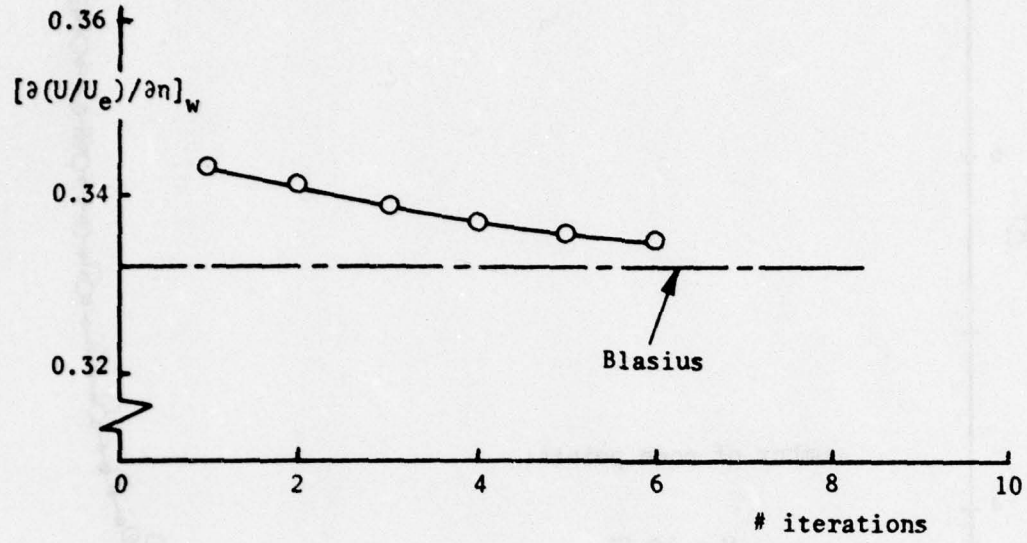

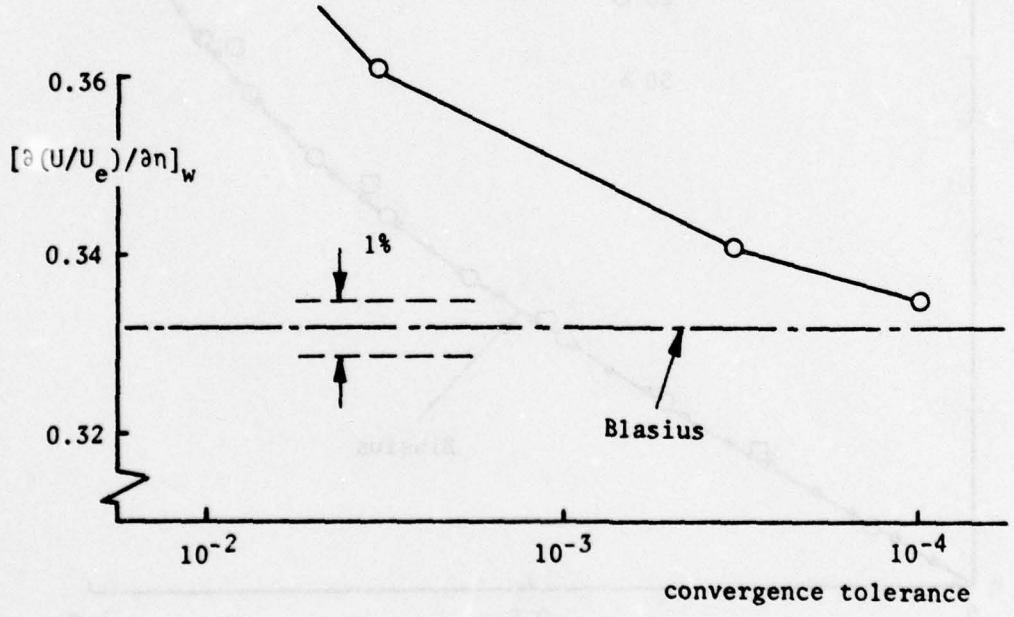

Figure 13 CONVERGENCE OF THE ITERATION PROCESS

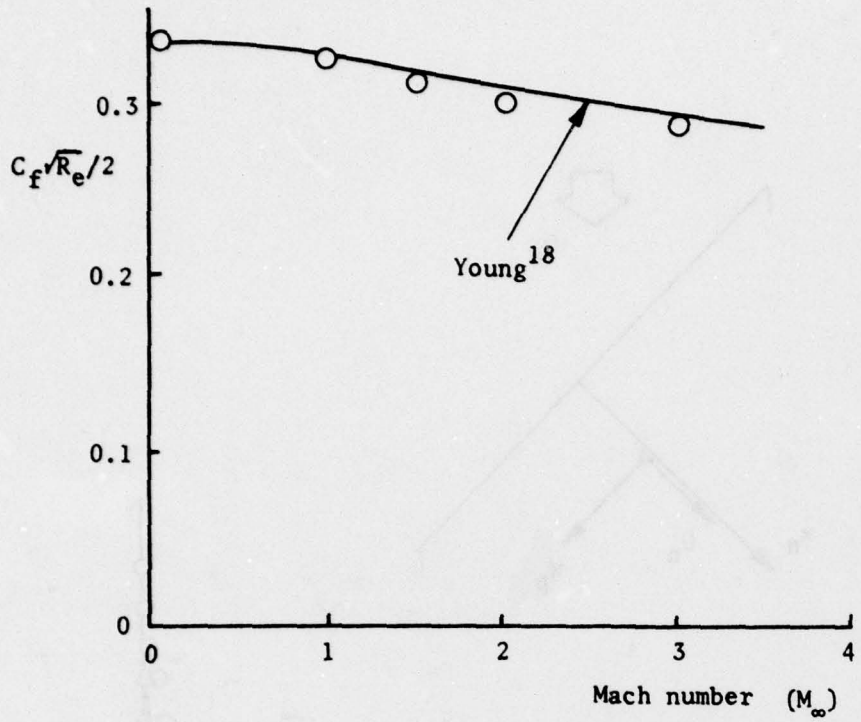

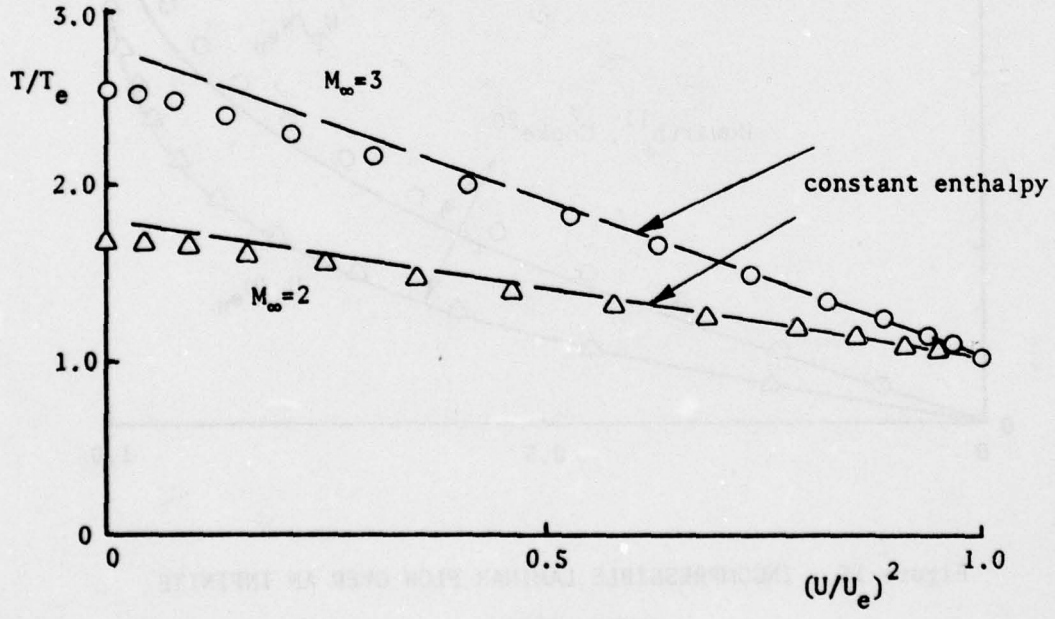

Figure 14 TWO-DIMENSIONAL, COMPRESSIBLE LAMINAR FLOW OVER A FLAT PLATE: WALL SHEAR STRESS, AND TEMPERATURE PROFILES

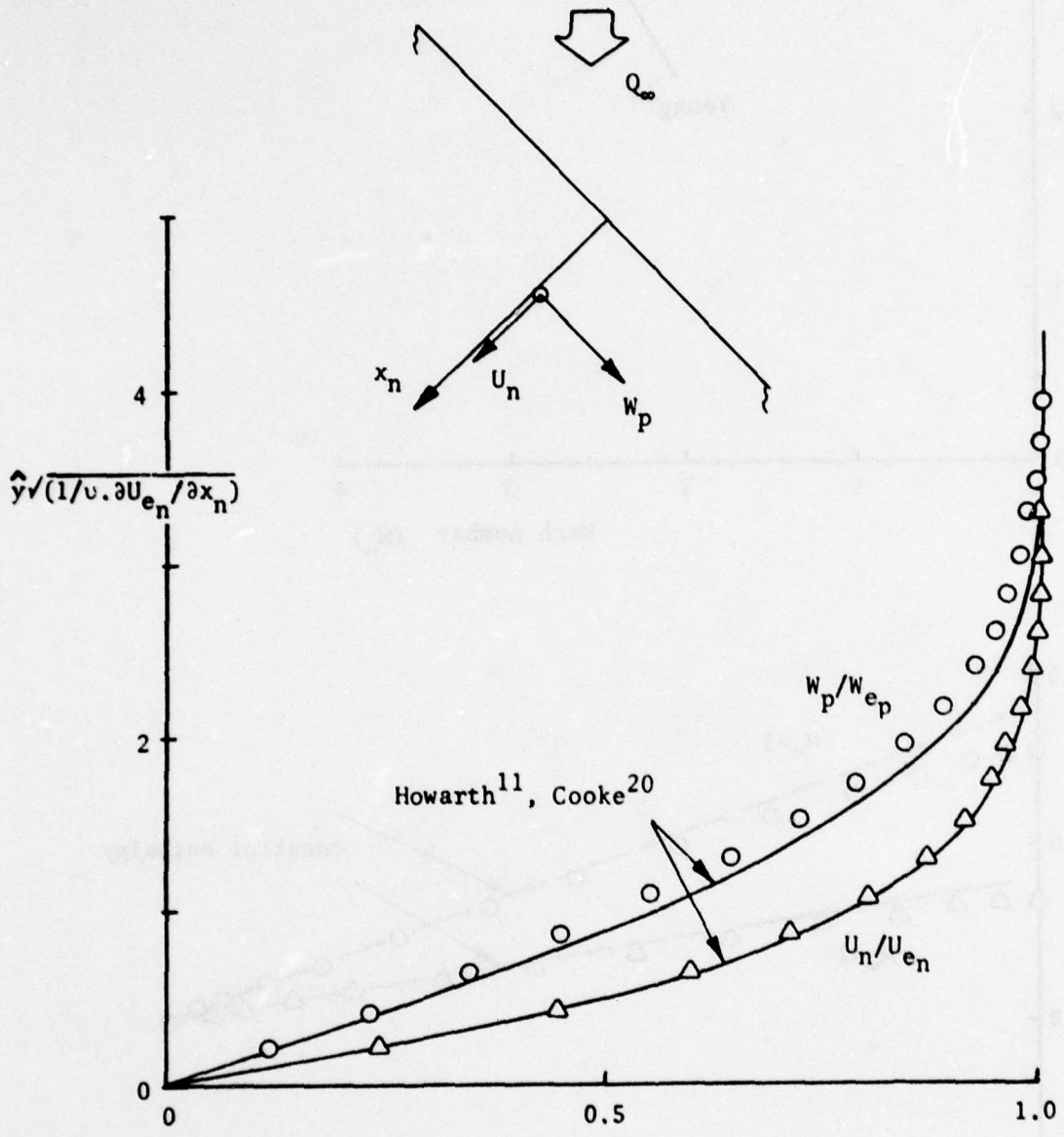

Figure 15 INCOMPRESSIBLE LAMINAR FLOW OVER AN INFINITE SWEPT WEDGE

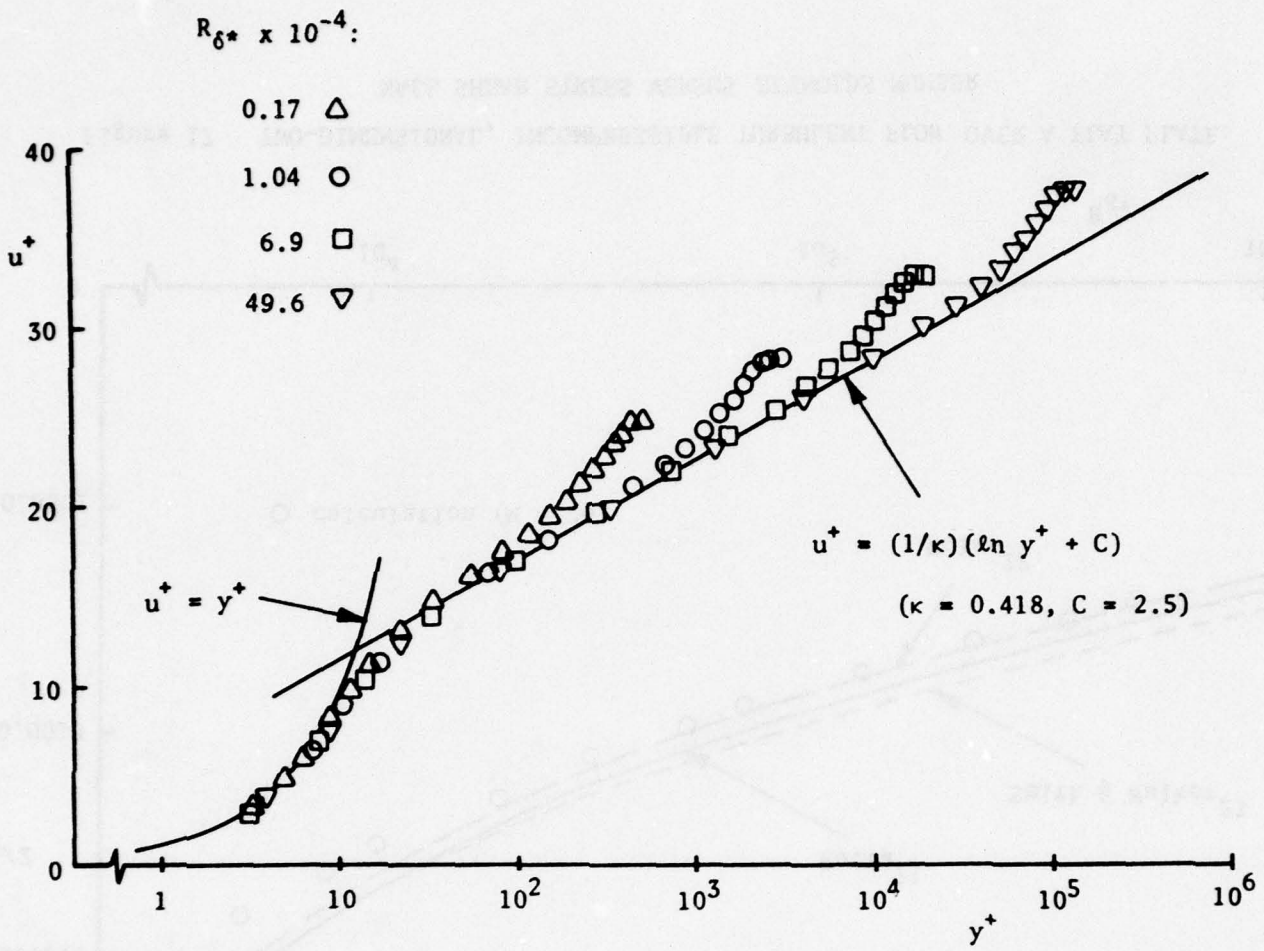

Figure 16 TWO-DIMENSIONAL, INCOMPRESSIBLE TURBULENT FLOW OVER A FLAT PLATE: VELOCITY PROFILES ON AN INNER-LAW PLOT

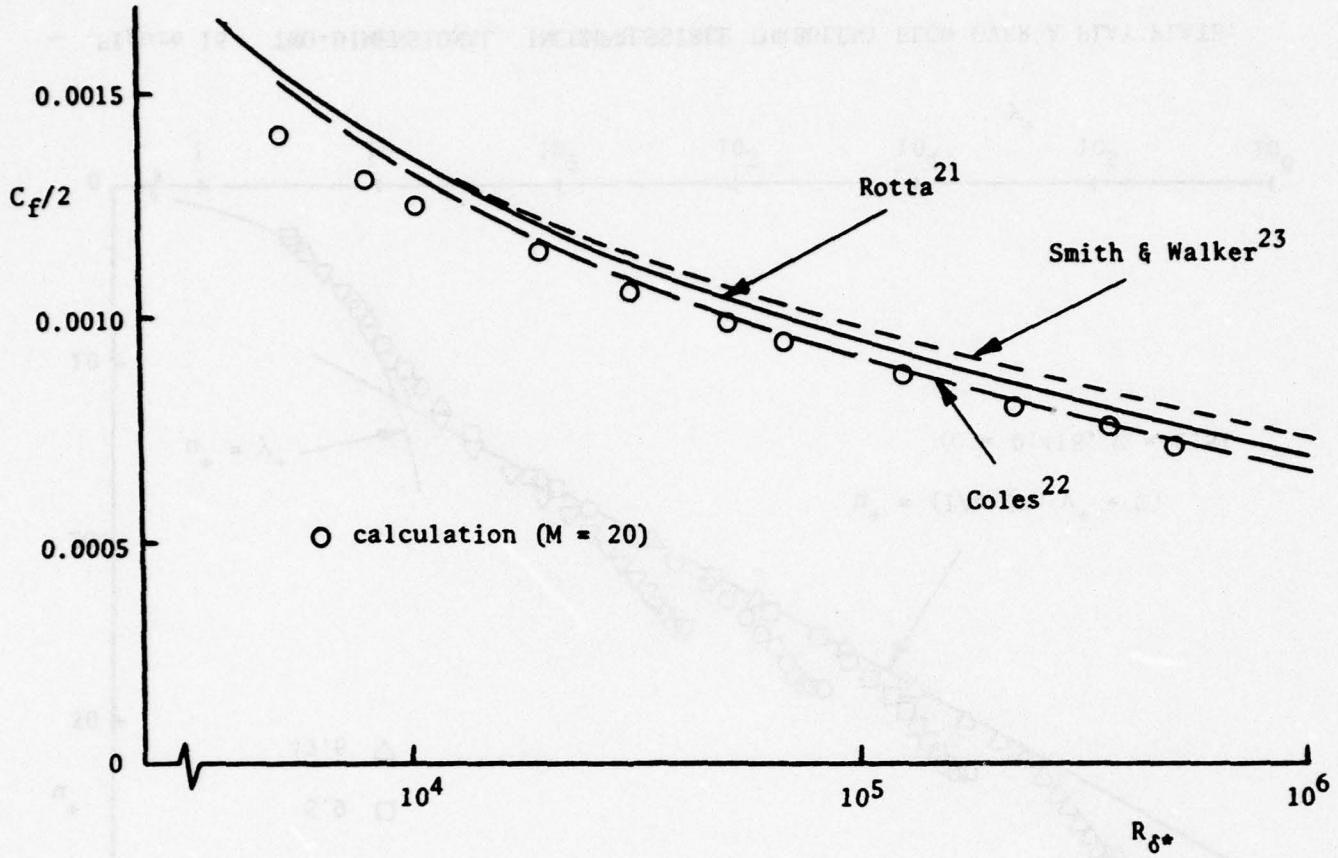

Figure 17 TWO-DIMENSIONAL, INCOMPRESSIBLE TURBULENT FLOW OVER A FLAT PLATE: WALL SHEAR STRESS VERSUS REYNOLDS NUMBER

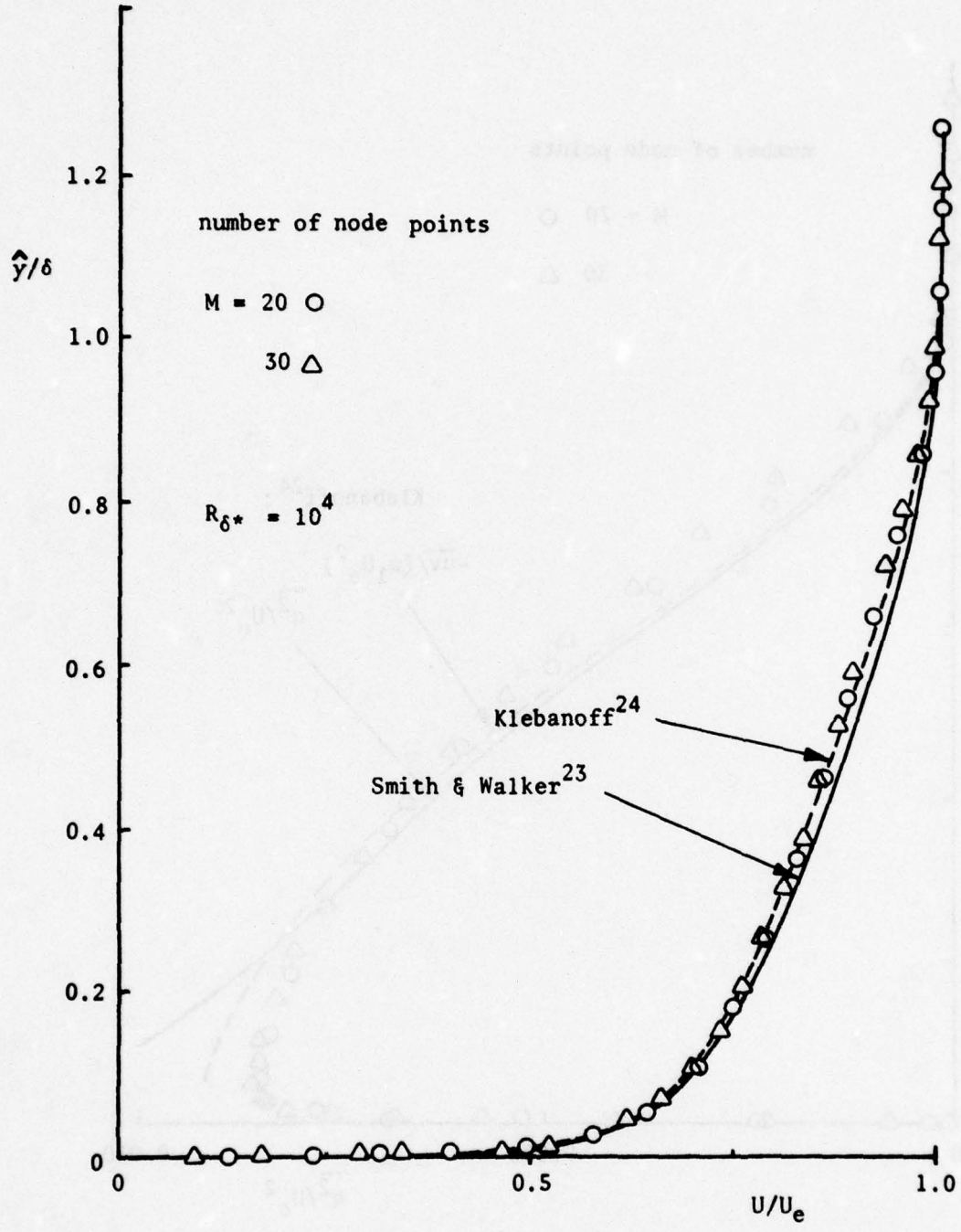

Figure 18 TWO-DIMENSIONAL, INCOMPRESSIBLE TURBULENT FLOW OVER A FLAT PLATE: VELOCITY PROFILE

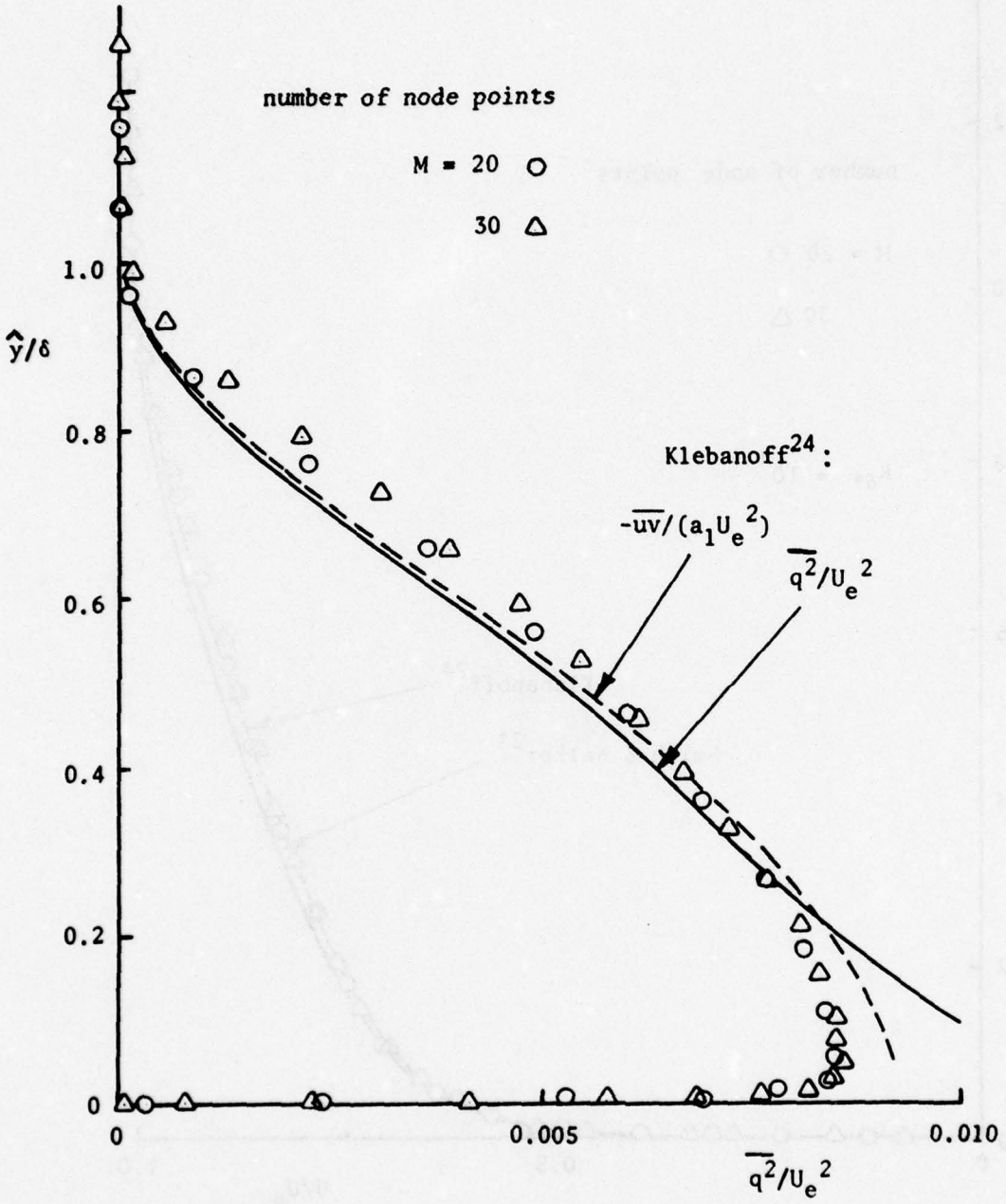

Figure 19 TWO-DIMENSIONAL, INCOMPRESSIBLE TURBULENT FLOW OVER A FLAT PLATE: PROFILE OF TURBULENT INTENSITY

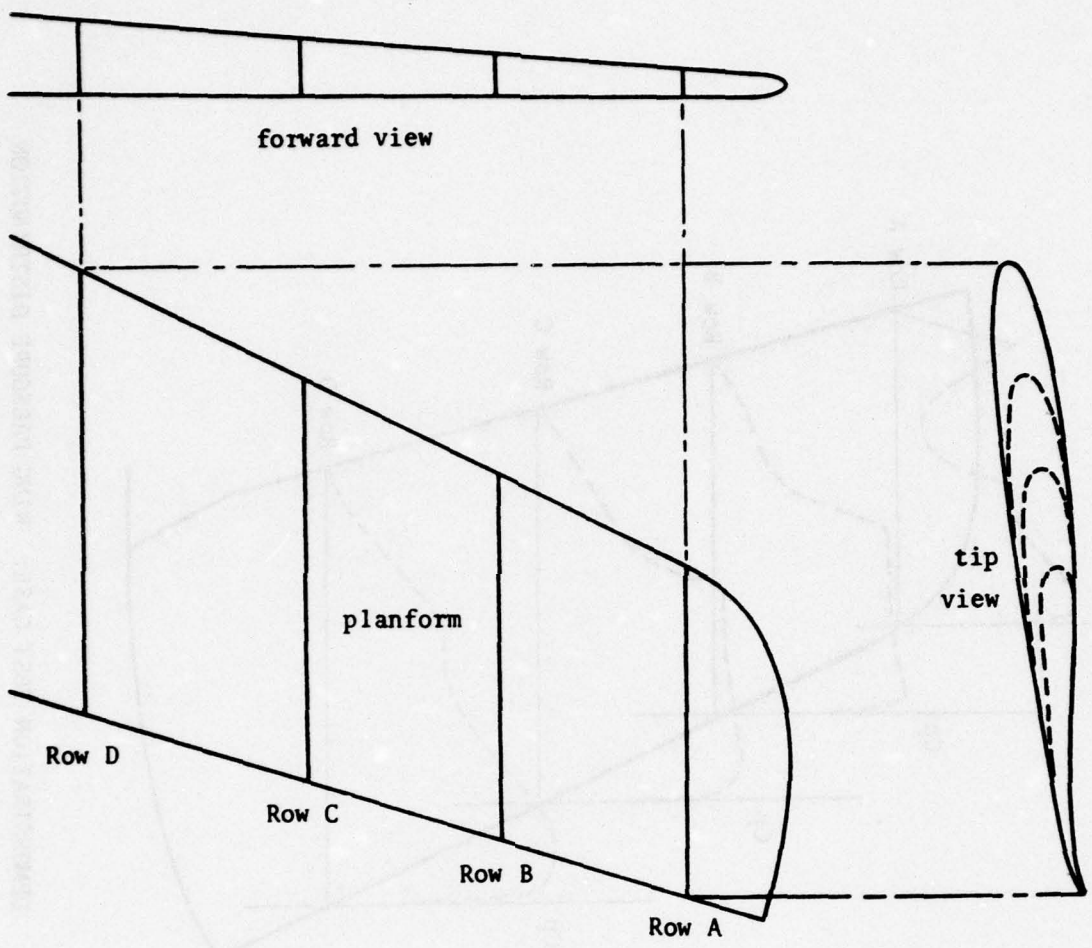

Figure 20 DEMONSTRATION TEST CASE: WING GEOMETRY

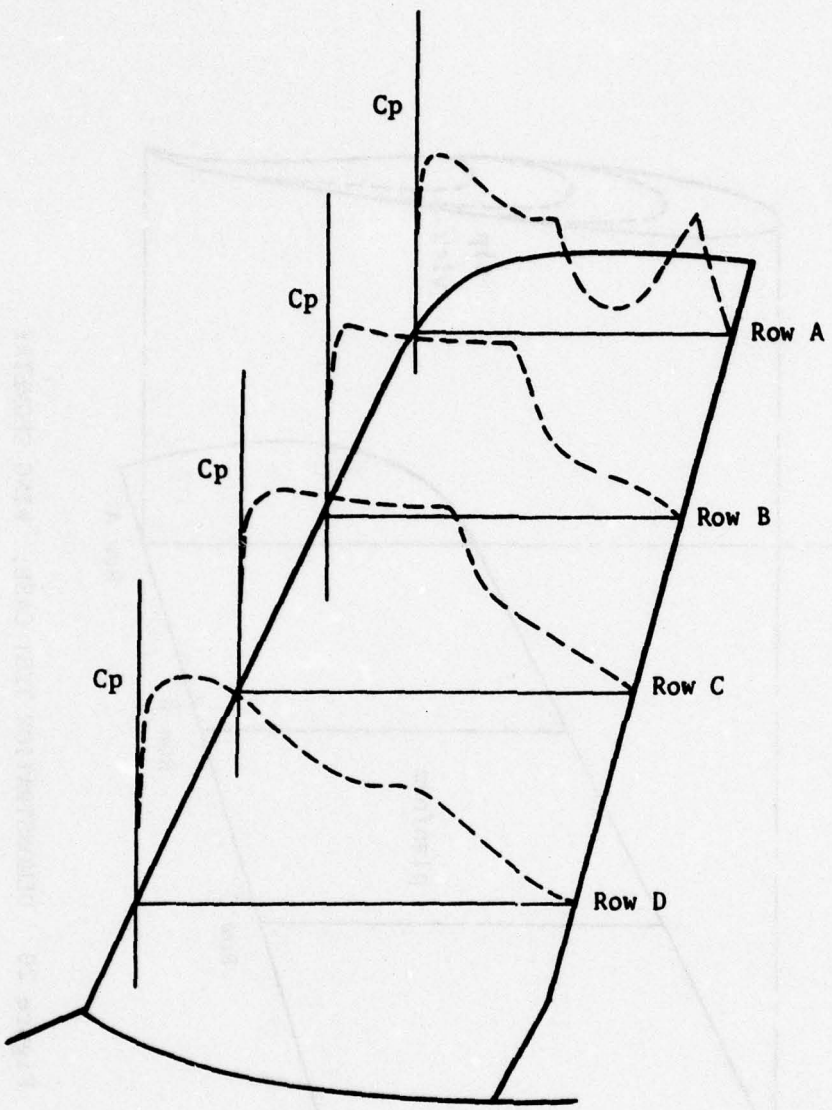

Figure 21 DEMONSTRATION TEST CASE: WING PRESSURE DISTRIBUTION

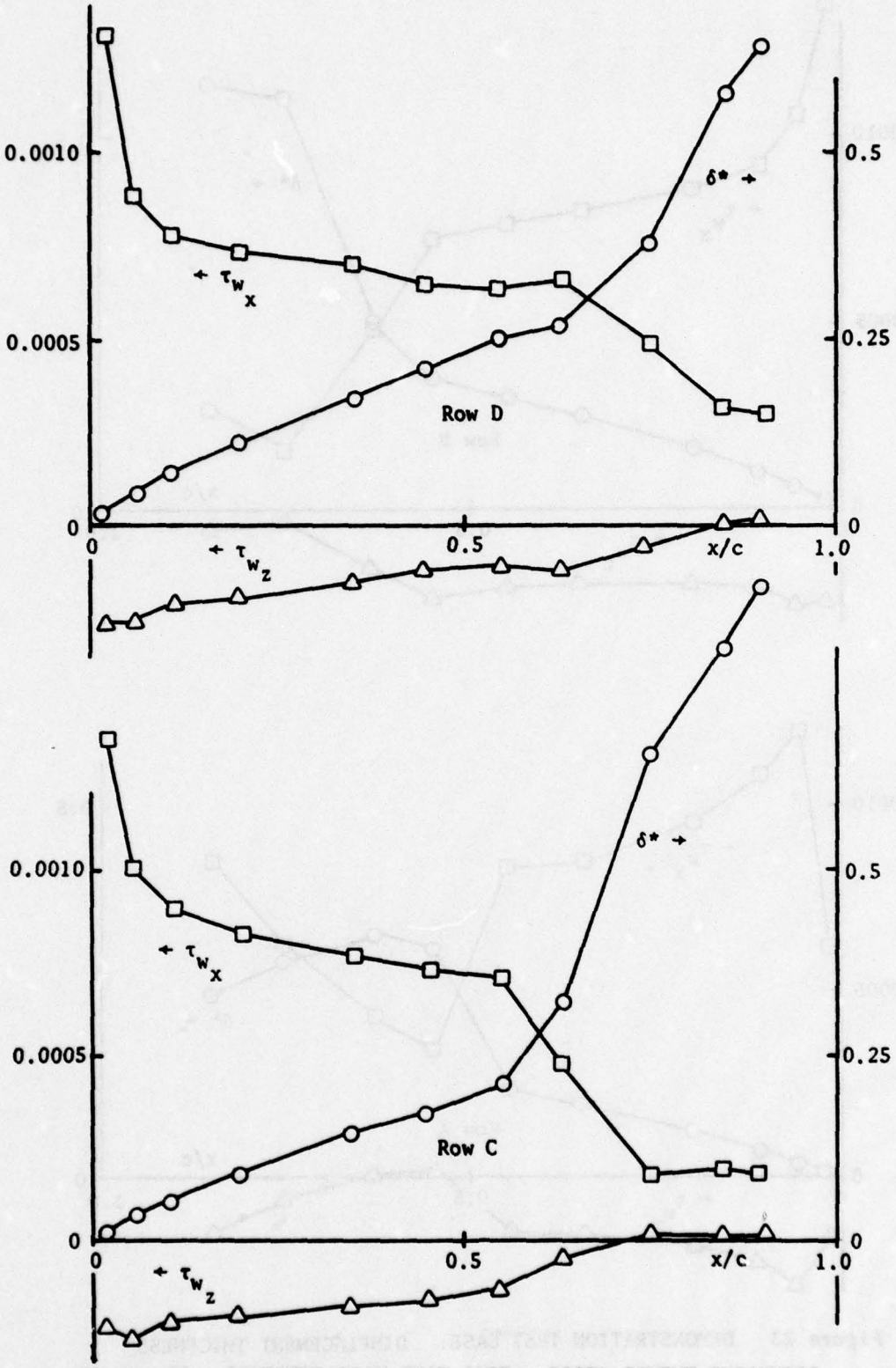

Figure 22 DEMONSTRATION TEST CASE: DISPLACEMENT THICKNESS AND WALL SHEAR STRESS -- ROWS D AND C

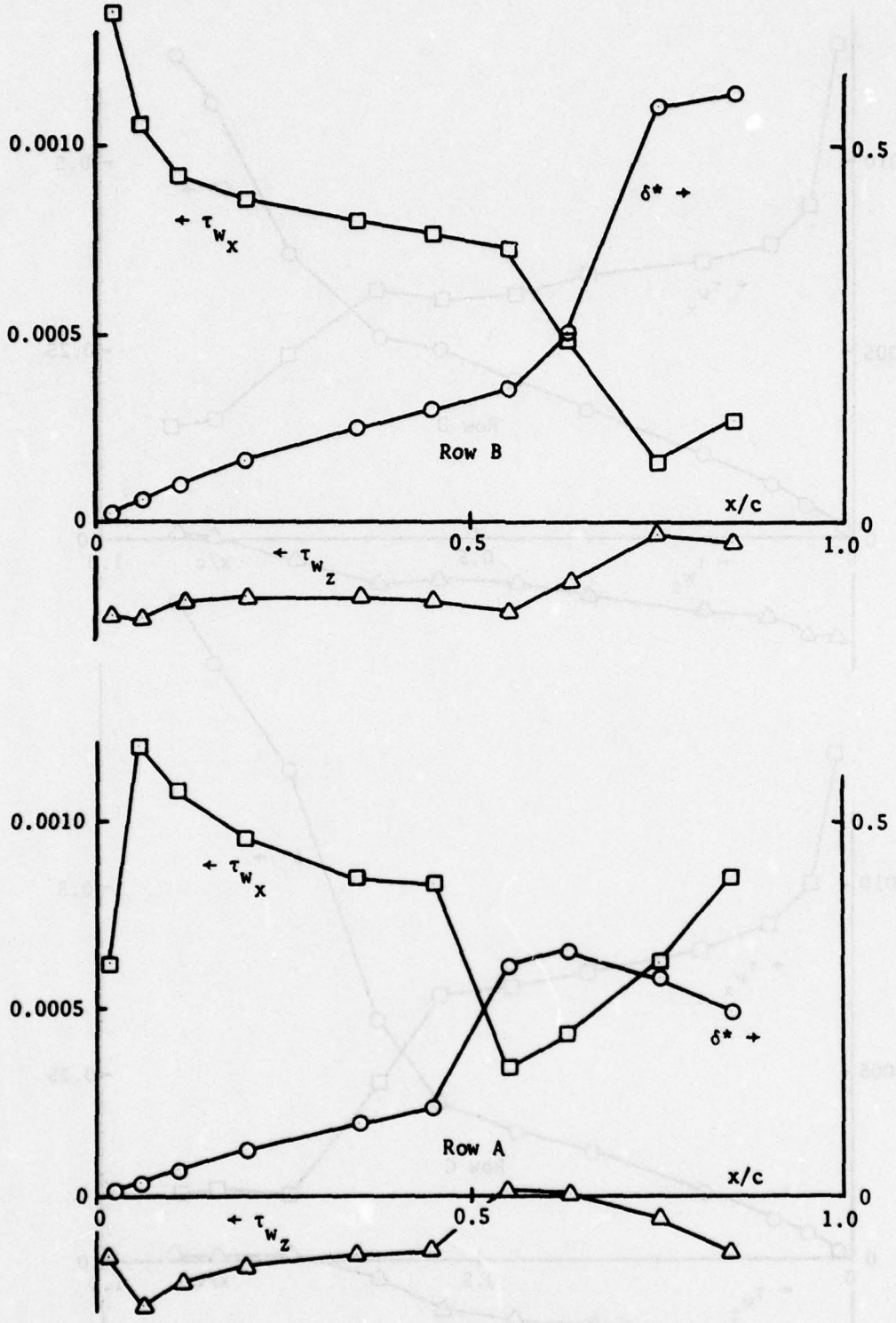

Figure 23 DEMONSTRATION TEST CASE: DISPLACEMENT THICKNESS AND WALL SHEAR STRESS -- ROWS B AND A

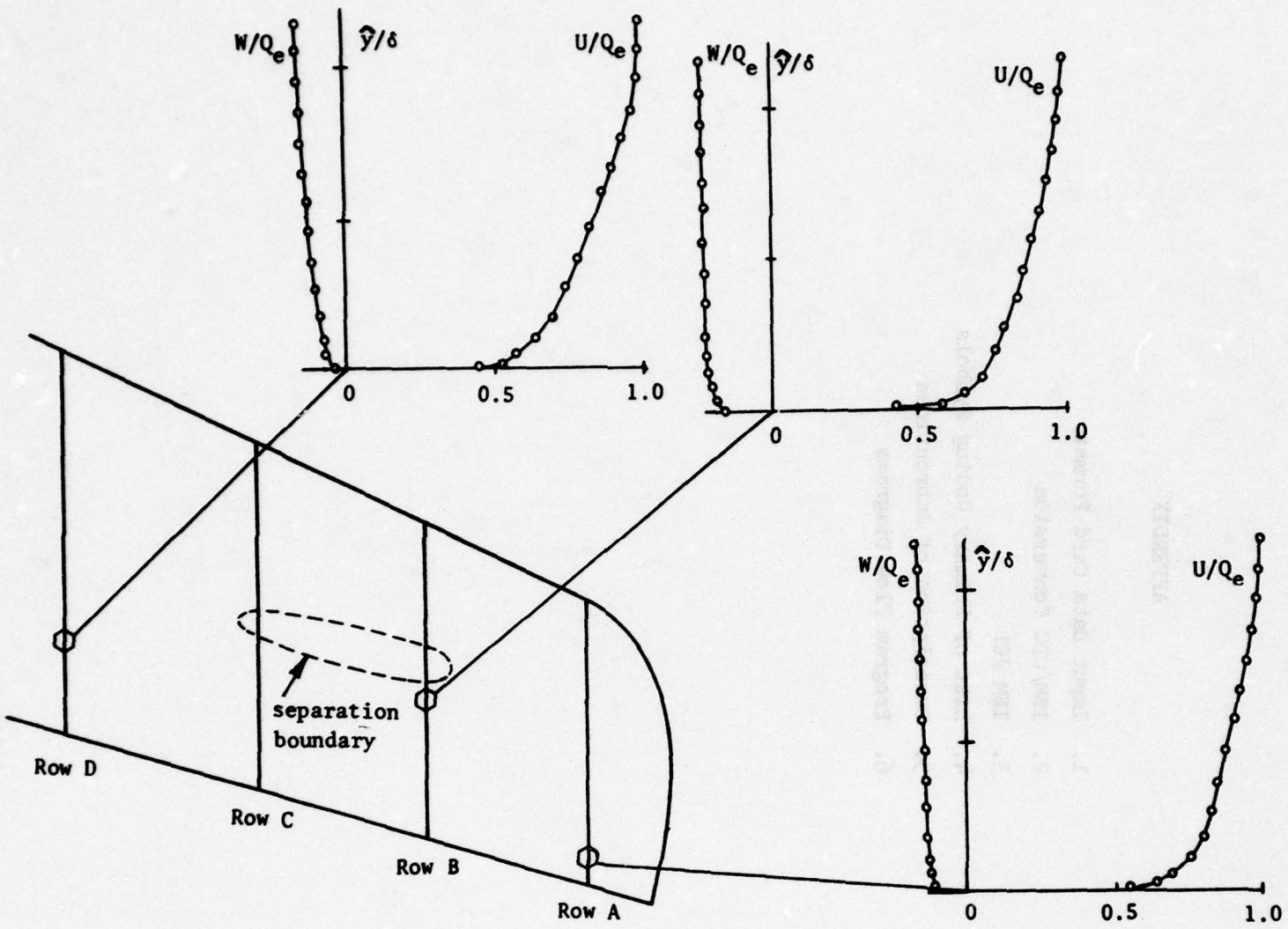

Figure 24 DEMONSTRATION TEST CASE: VELOCITY PROFILES

APPENDIX

1. Input Data Card Format
2. IBM/CDC Conversion 5
3. IBM JCL
4. List of Primary Coding Symbols
5. Description of Subroutines
6. Program Flow Diagrams

NASH/SCRUGGS THREE DIMENSIONAL BOUNDARY LAYER CODE*

Input Procedure

The input data is contained in several blocks. All input is read into the MAIN program added at Grumman.

Card #	Format	Field	Name	Remarks
A1	Literal	-	GTITLE1	1st card of 2 card title set (STOP in the 1st 4 columns terminates execution)
A2	Literal	-	GTITLE2	2nd card of 2 card title set
A3	21I3	1	LL	# of streamwise stations (≤50)
		2	MM	# of computational points across boundary layer (<21)
		3	NN	# of span stations (<30)
		4	ITN	Maximum number of iterations allowed in numerical procedure at each streamwise row
A4	21I3	1	KBC	Edge boundary conditions
				=1 2-D flow
				=2 plane-of-symmetry flow
				=3 infinite yawed-wing flow
		2	IOITER	Output of numerical iteration history
				=0 no output
				=1 full output
		3	IOPRF	Output of velocity profiles at each station
				=0 no output
				=1 full output

* Input format revised slightly by Bill Mason at Grumman, where this section was rewritten.

BLOCK B Geometry Input

Card #	Format	Field	Name	Remarks
B1	7F10.0	1	XXGEOM(N,1)	X (streamwise) location of leading edge at span station N
		2	XXGEOM(N,2)	Y (vertical) location of leading edge at span station N
		3	XXGEOM(N,3)	Z (span) location of leading edge at span station N
		4	XXGEOM(N,4)	Local chord at span station N
		5	XXGEOM(N,5)	Wing incidence (in addition to ordinates) at span station N
B2	7F10.0	1→LL	XYGEOM(L1,N,1)	$(\frac{x}{c})$ ordinates at span station N, read for L1 from 1 to LL

NOTE: Card B2 is read seven values per card until LL values are read.

B3	7F10.0	1→LL	XYGEOM(L1,N,2)	$(\frac{y}{c})$ ordinates at span station N, read for L1 from 1 to LL

NOTE: Card B3 is read seven values per card until LL values are read.

NOTE: BLOCK B is repeated once for each span station starting with the most inboard span station (NN times).

BLOCK C Flight Conditions

C1	Literal		TITLE	Title card describing flight condition and pressure distribution.
C2	7F10.0	1	XMINF	Mach number
		2	XLEN	Reference length scale, in feet
		3	PINF	Static pressure, in psi
		4	TINF	Static temperature, in degrees Rankine
C3	21I3	1→NN	LTRN(N)	Chordwise location of specified transition at each span station

NOTE: Card C3 is read a second time if NN > 21.

Card #	Format	Field	Name	Remarks
C4	21I3	1	KWTF	= 0 do not write solution to file
				= 1 write solution to file
		2	KRFF	= 0 do not read solution from file
				= 1 read solution from file
		3	IPNCH	= 0 do not punch output for plotting
				= 1 punch output for plotting
		4	KSMTHS	Number of smoothings of input pressure distribution (if desired)
C5	7F10.0	1	CNCRIT	Convergence criterion for numerical iteration (.0005 nominal value)
		2	CRTLAM	Separation test for laminar flow (.05 nominal value)
		3	CRTTBL	Separation test for turbulent flow (.005 nominal value)

BLOCK D Pressure Distribution

D1	7F10.0	1→LL	CP(L,N)	Pressure distribution at constant span station, L.E. to T.E.

NOTE: Card D1 is read repeatedly until LL values are input, seven values per card.

NOTE: BLOCK D is read once for each span station (NN times).

Program Termination: The program will automatically return to the beginning and read card A1. If the 1st 4 columns in Card A1 contain the clue work STOP, execution terminates.

IBM/CDC Conversion

Only minor modifications are required to convert the program from CDC to IBM or vice versa. The following list provides the entire details of the conversion procedure.

I. Comment out the program cards for IBM.

II. Entry points must be changed. These occur in the listed subroutines:

	SUBROUTINE	CDC	IBM
1.	BOUND	ENTRY GUESS	ENTRY GUESS (L)
2.	PRINT	ENTRY PRINT2	ENTRY PRINT2(L)
3.	PRINT	ENTRY PRINT3	ENTRY PRINT3(L)
4.	DISP	ENTRY DISP2	ENTRY DISP2(L)
5.	GEOMT	ENTRY GEOM2	ENTRY GEOM2(L)

III. For those IBM installations that do not have the H-Extended Compiler, two function subprograms are required in order to supply ASIN and ACOS. This is done by using the function subprograms to equate ASIN to ARSIN and ACOS to ARCOS.

IBM JCL

```
//GRUM0001 JOB (7278,I36,0050,0030,0000,,2,,62),'MACKENZIE-575-5722',  X
//     MSGLEVEL=1,CLASS=C,REGION=256K,TIME=15
/*MESSAGE  CPU TIME 15 MIN, WALL CLOCK  50 MIN, REGION 256K
//NASH EXEC FORTHCLG,PARM.FORT='OPT=2',REGION.FORT=256K,                X
//     PARM.LKED='SIZE=(110K,285),MAP,LET,LIST',                        X
//     TIME.GO=15
//FORT.SYSLIN DD DSN=&&LOADSET,DISP=(,PASS),                            X
//     UNIT=(SYSDA,SEP=SYSPRINT),SPACE=(CYL,(4,1)),                     X
//     DCB=(RECFM=FB,LRECL=80,BLKSIZE=3200)
//FORT.SYSIN DD DISP=SHR,DSN=D770278.MASON.GACNASH.CARDS,               X
//     UNIT=3330,VOL=SER=OSPF02
//LKED.SYSIN DD *
  ENTRY MAIN
/*
//GO.FT07F001 DD DUMMY
//GO.FT14F001 DD UNIT=SYSDA,SPACE=(CYL,(2,1)),DISP=(,DELETE),          X
//     DCB=(RECFM=VBS,LRECL=32,BLKSIZE=704)
//GO.FT15F001 DD DUMMY
//GO.FT16F001 DD UNIT=SYSDA,SPACE=(TRK,(8,5)),DISP=(,DELETE),          X
//     DCB=(RECFM=VBS,LRECL=52,BLKSIZE=96)
//GO.SYSIN DD *
    (CARD INPUT GOES HERE)
/*
```

1. List of Primary Coding Symbols

Indices:

M index in the y-direction, MM upper limit.
N index in the z-direction, NN upper limit.
L index in the x-direction, LL upper limit.
IT iteration number, upper limit ITN.

F(M,N,1)	U(y,z)
F(M,N,2)	W(y,z)
F(M,N,3)	T(y,z)
F(M,N,4)	$\overline{q^2}(y,z)$
FO(M,N,I)	the quantities above, I = 1,4, for the previous x-station. (In general an "O" appended will have this meaning.)
FP(M,N,I)	values of F(M,N,I) from previous iteration
CP(L,N)	$C_p(x,z)$
H1(N)	metric coefficient h_1.
H3(M,N,I)	metric coefficient h_3, measured on the side of increasing z (I = 1) and on the side of decreasing z (I = 2) at local development point.
DISP(N)	displacement thickness
LAMINAR(N)	equals 1 for laminar flow, 2 for turbulent flow.
LTRN(N)	value of L for which transition is specified, at each N. (input)
KBC	an integer fixing boundary conditions in the z-direction. (input)
QE(N)	velocity at the edge of the boundary layer.
RHOE(N)	density at edge of the boundary layer.
ROT1(N,I,J)	rotation matrix for the side of decreasing z at the local development point (I,J = 1,4).
ROT2(N,I,J)	same as ROT1 for left hand side.
SWP(N)	leading edge sweep angle.
ROB(N,I,J)	backward rotation matrix at the local development point

SWPL(N)	local sweep angle.
XME(N)	Mach number at edge of the boundary layer.
XK13(N,I)	the curvature coefficient K_{13}, measured on the side of decreasing z (I = 2), and on the side of increasing z (I = 4) at the local development point.
V(M,N)	$\rho V + \overline{\rho' v}$
XK2(M,N,I)	the curvature coefficient K_{22} for the previous x-level (I = 1) and the current x-level (I = 2).
XR(N,I)	the quantity λ measured on the side of decreasing z (I = 2) and on the side of increasing z (I = 4), at the local development point.
YDELTA(N)	boundary layer thickness at each z-station.
Y(M,N)	curvilinear coordinate normal to body surface.

2. Description of Subroutines

The flow diagrams in Figure A1 through A4 describe the sequence of events in the computer code. Basically, the code is built around a driver program called MAIN, which sequences most of the activity given in the diagrams. All computations are performed through a series of subroutines and functions. Following is a brief narrative on each of these.

BOUND (L).

At each x-station computes local edge conditions for each z-station and local pressure gradients (transformed) in the x and z directions. Linearly extrapolates boundary layer thickness from previous x-station for each z. Forms a "best guess" set of profiles to start iteration process at the current x-station by scaling the converged solution from the previous x-station (entry point GUESS).

CONT.

Computes boundary layer thickness, maximum turbulence intensity, and wall shear stress for each z, on each iteration. Solves continuity equation for normal velocity V.

DISP(L).

Computes displacement thickness for each z-station from the differential equation given in the text.

EQTNS.

Computes the 4 x 4 coefficient matrices A_1 through A_6 given in Equation (2.32) through (2.57). These coefficients are updated on each iteration. This subroutine is called from SETUP.

FUNCT.

Forms a function used to generate certain matrix elements in EQTNS.

GEOMT(L).

Loft data are entered in this subroutine and all geometric functions are computed for each surface point. The quantities are generated at z^+ and z^- as appropriate, and taking account at the ends the necessary values for infinite swept or plane-of-symmetry conditions. Leading edge and local sweep angles are also computed. Rotation matrices are generated at each z-station for z^+ and z^-, for vector transfer in the z-direction. Rotation matrices are also formed at each z for vector transfer in the x-direction. These calculations are performed for each x-station in succession and stored on tape. The entry point GEOM2 then returns the data row-wise for the marching procedure in the main program.

INITV.

Computes flow conditions along the swept leading edge. Applies criteria to determine whether turbulent or laminar flow conditions are to be applied. Starting profiles for the vector F are generated accordingly.

INPUT.

Reads input conditions from cards and computes appropriate constants of the flow.

INVRT(A,B,ID).

Computes the inverse of a 4 x 4 matrix. Inverse of A returned in B. ID = 0 returns singularity condition. This subroutine is called in SOLVE.

MULT4(A,B,C,JJ).

Product of matrices A and B returned in C. Matrices are 4 x JJ.

Called in SETUP and SOLVE.

PRINT(L).

Prints solution profiles in x and z, stream and normal, forms. Computes and prints wall shear stresses, prints boundary layer thickness and displacement thickness. Also prints iteration history of the solution.

SCALE.

Used on first x-step away from the leading edge to scale the solution back to the attachment line.

SEPCON(L).

This subroutine is called when, for any z-station, the given pressure gradients cause separation to occur. The solution cycle then passes through SEPCON successively until a decreased adverse gradient is found which allows the iteration cycle to be completed for the given x-station. The local adverse gradient is decreased linearly on each pass.

SETUP.

Sets up the tri-diagonal matrix, each of whose elements is a 4 x 4 matrix. EQTNS is called to form the A_1 through A_6 matrices at each mesh point. These are then loaded appropriately in the elements of the tri-diagonal system.

SOLVE.

Performs inversion for the tridiagonal. Called from SETUP. Returns a solution of the system of equations for F on each iteration.

STORE.

Called on each x-step. Converged solution for current x-step is stored. In addition this solution is rotated to the coordinate system

for the next x-step, for each z-station. Entry point STOR2 writes the solution to tape.

YPOINT(KINT).

Generates a distribution of mesh points in the y-direction and computes appropriate geometric terms for this coordinate, i.e. h_2, k_{22}, and their derivatives. KINT $\neq$ 0 interpolates the solution F to the new distribution of points.

ZDERV.

The function ZDERV performs z-derivatives of any quantity, scalar or vector, one-sided or centered, and which may be defined at some or all of the six local developments points associated with the point where the derivative is taken.

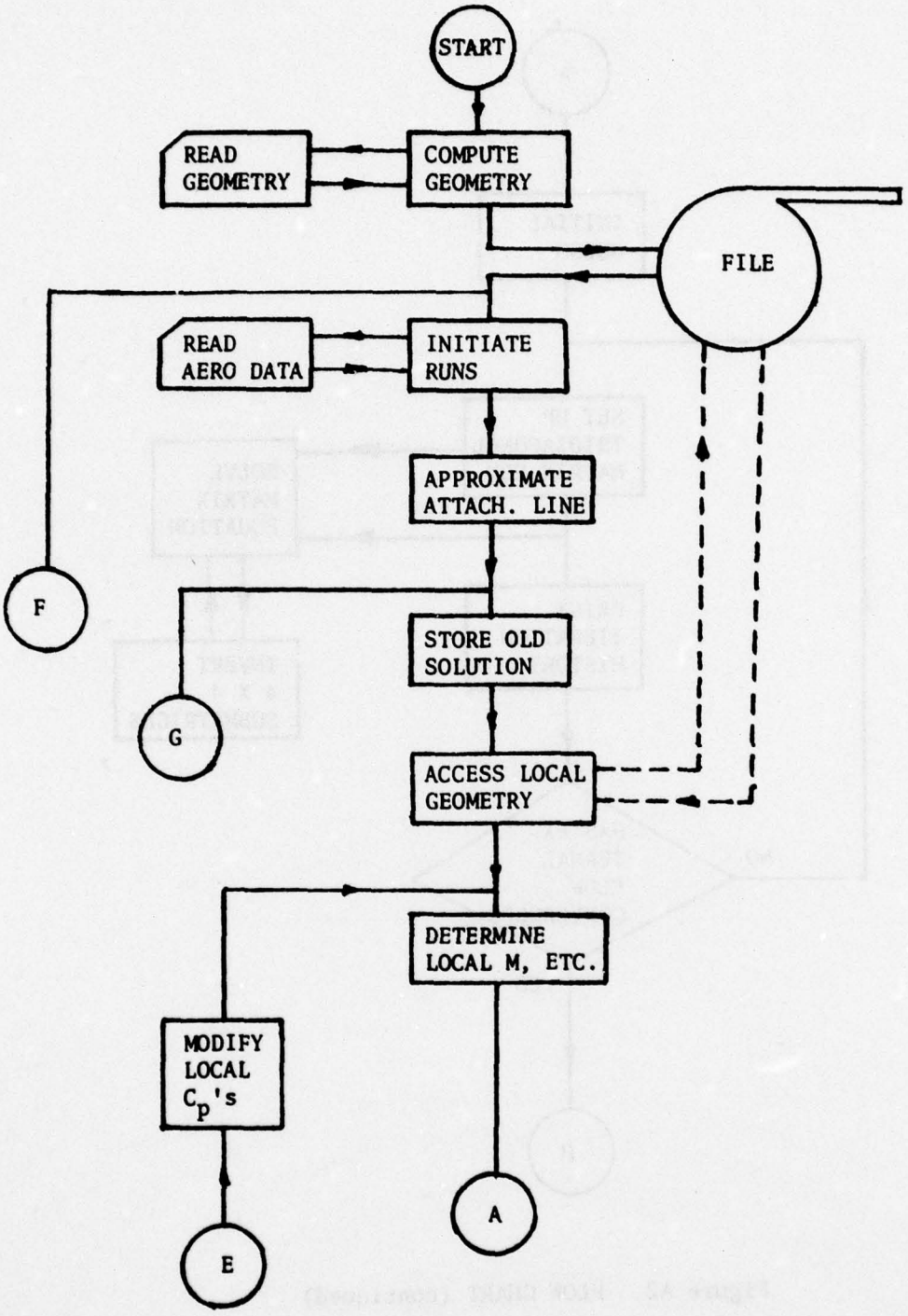

Figure A1 FLOW CHART OF THE CALCULATION METHOD

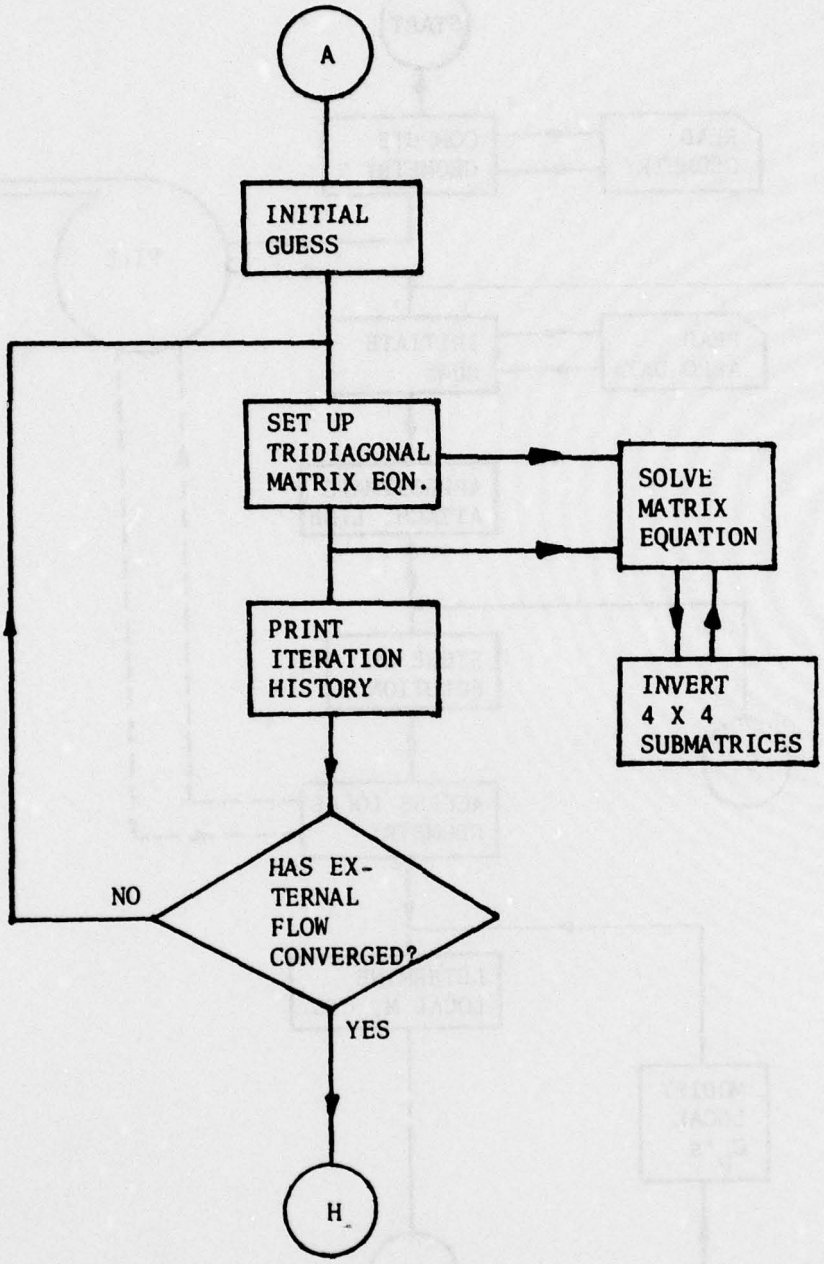

Figure A2 FLOW CHART (continued)

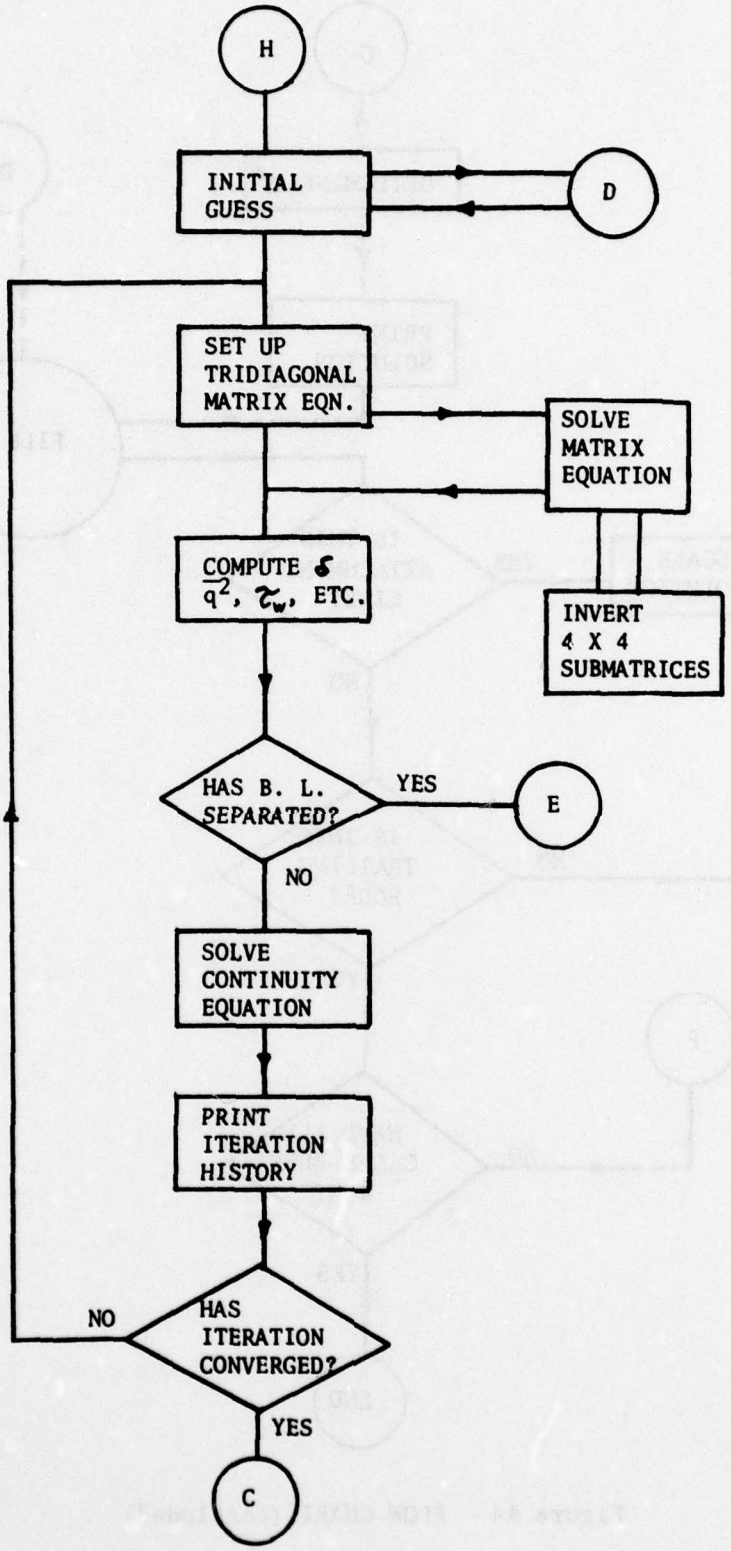

Figure A3 FLOW CHART (continued)

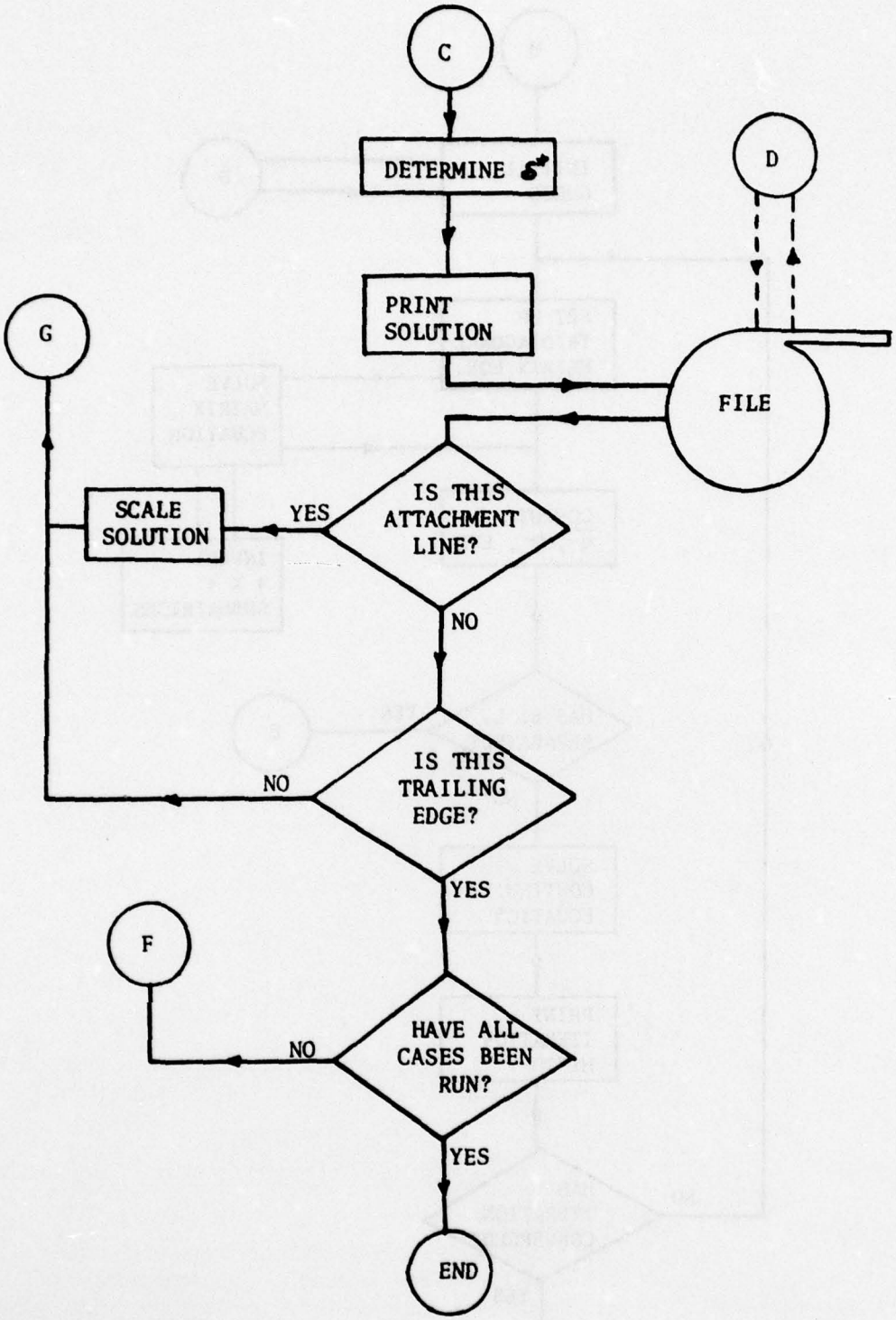

Figure A4 FLOW CHART (concluded)

REFERENCES

1. J. F. Nash (1969), "The Calculation of Three-Dimensional Turbulent Boundary Layers in Incompressible Flow," J. Fluid Mech. 37, part 4, p. 625.

2. J. F. Nash (1972), "An Explicit Scheme for the Calculation of Three Dimensional Turbulent Boundary Layers," J. Basic Eng. 94D, No. 1, p. 131.

3. J. F. Nash and V. C. Patel (1971), "A Generalized Method for the Calculation of Three-Dimensional Turbulent Boundary Layers," Project SQUID Symposium, Georgia Institute of Technology.

4. J. F. Nash and V. C. Patel (1972), Three-Dimensional Turbulent Boundary Layers, SBC Technical Books.

5. J. F. Nash and R. R. Tseng (1971) "The Three-Dimensional Turbulent Boundary Layer on an Infinite Yawed Wing," Aero. Quart. 22, p. 346.

6. J. F. Nash and R. M. Scruggs (1972), "Three-Dimensional Compressible Boundary Layer Computations for a Finite Swept Wing," NASA CR-112158.

7. J. F. Nash, R. M. Scruggs, and W. A. Stevens (1973), "Additional Three-Dimensional Boundary-Layer Computations for a Finite Swept Wing," NASA CR-132335.

8. J. G. Hicks and J. F. Nash (1971), "The Calculation of Three-Dimensional Turbulent Boundary Layers on Helicopter Rotors," NASA CR 1845.

9. L. P. Eisenhart (1909), "A Treatise on the Differential Geometry of Curves and Surfaces," Dover Publications.

10. P. Bradshaw (1968), "Calculation of Boundary-Layer Development using the Turbulent Energy Equation: IV Heat Transfer with Small Temperature Differences," Nat. Phys. Lab. Rep. Aero. 1271.

11. P. Bradshaw, D. H. Ferriss, and N. P. Atwell (1967), "Calculation of Boundary-Layer Development Using the Turbulent Energy Equation," J. Fluid Mech. 28, part 3, p. 593.

12. A. A. Townsend (1956), The Structure of Turbulent Shear Flow, Cambridge University Press.

13. N. A. Cumpsty and M. R. Head (1969), "The Calculation of Three-Dimensional Turbulent Boundary Layers. Part III: Comparison of Attachment Line Calculations with Experiment," Aero. Quart. 20, p. 99.

14. L. Rosenhead (Ed.) (1963), Laminar Boundary Layers, Clarendon Press, Oxford.

15. M. J. Lighthill (1958), "On Displacement Thickness," J. Fluid Mech., 4, p. 383.

16. W. R. Briley, H. McDonald, and H. J. Gibeling (1976), "Solutions of the Multidimensional Compressible Navier-Stokes Equations by a Generalized Implicit Method," United Technologies Research Center, Final Report R75-911363-15, Contract N00014-72-e-0183.

17. R. D. Richtmyer and K. W. Morton, Difference Methods for Initial-Value Problems, Wiley, 1967.

18. A. D. Young and T. B. Booth (1951), "The Profile Drag of Yawed Wings of Infinite Span," Aero. Quart. 3, p. 211.

19. L. Howarth (1951), "The Boundary Layer in Three-Dimensional Flow. Part II: The Flow Near a Stagnation Point," Phil. Mag. (7) 42, p. 1433.

20. J. C. Cooke (1950), "The Boundary Layer of a Class of Infinite Yawed Cylinders," Proc. Camb. Phil. Soc. 46, p. 654.

21. J. C. Rotta (1962), "Turbulent Boundary Layers in Incompressible Flow," Progress in Aeronautical Science, Pergamon Press.

22. D. Coles (1955), "The Law of the Wall in Turbulent Shear Flow," 50 Jahre Grenzschichtforschung, Vieweg & Sohn.

23. D. W. Smith and J. H. Walker (1959), "Skin-Friction Measurements in Incompressible Flow," NASA TR R-26.

24. P. S. Klebanoff (1955), "Characteristics of Turbulence in a Boundary Layer with Zero Pressure Gradient," N.A.C.A. Rep. No. 1247.

25. V. C. Patel, A. Nakayama, and R. Damian (1973), "An Experimental Study of the Thick Turbulent Boundary Layer Near the Tail of a Body of Revolution," Inst. of Hydraulic Research, Rept. No. 142.

26. P. Bradshaw (1967), "The Turbulence Structure of Equilibrium Boundary Layers," J. Fluid Mech. 29, p. 625.

27. P. Bradshaw and D. H. Ferriss (1965), "The Response of a Retarded Equilibrium Turbulent Boundary Layer to the Sudden Removal of Pressure Gradient," Nat. Phys. Lab. Aero. Rep. 1145.

*U.S.Government Printing Office: 1978 — 757-080/541